THE ASTROPHYSICAL JOURNAL, 489:719–733, 1997 November 10


# A SEARCH FOR INFALL MOTIONS TOWARD NEARBY YOUNG STELLAR OBJECTS

D. MARDONES, P. C. MYERS, M. TAFALLA, AND D. J. WILNER[1]
Harvard-Smithsonian Center for Astrophysics, 60 Garden Street, Cambridge, MA 02138
R. BACHILLER
Observatorio Astronómico Nacional, Apartado 1143, E-28800 Alcalá de Henares, Spain
AND
G. GARAY
Universidad de Chile, Casilla 36-D, Santiago, Chile
*Received 1997 February 21; accepted 1997 June 23*

## ABSTRACT

We report observations of 47 candidate protostars in two optically thick lines [$H_2CO$ ($2_{12}$–$1_{11}$) and CS (2–1)] and one optically thin line [$N_2H^+$ (1–0)] using the IRAM 30 m, SEST 15 m, and Haystack 37 m radio telescopes. The sources were selected for the redness of their spectra ($T_{bol} < 200$ K) and their near distance ($d < 400$ pc). Most of the sources have asymmetric, optically thick lines. The observed distribution of velocity differences, $\delta V = (V_{thick} - V_{thin})/\Delta V_{thin}$, is skewed toward negative (blueshifted) velocities for both the $H_2CO$ and CS samples. This excess is much more significant for class 0 than for class I sources, suggesting that we detect infall motions toward class 0 and not toward class I sources. This indicates a difference in the physical conditions in the circumstellar envelopes around class I and class 0 sources, but it does not rule out the presence of infall onto class I sources by, for example, lower opacity gas. Bipolar outflows alone, or rotation alone, cannot reproduce these statistics if the sample of sources has randomly oriented symmetry axes. We identify 15 spectroscopic infall candidates, six of which are new. Most of these infall candidates have primarily turbulent rather than thermal motions and are associated with clusters rather than being isolated.

*Subject headings:* ISM: jets and outflows — ISM: kinematics and dynamics — ISM: molecules — radio lines: stars — stars: formation — stars: pre–main-sequence

## 1. INTRODUCTION

Low-mass stars form by gravitational collapse of dense cores in molecular clouds. The collapse is believed to proceed from a condensed initial state (Larson 1969; Shu 1977), with a rapid development of a system consisting of a protostellar core that accretes mass from a disk and envelope. This gravitational collapse model can now be explored through detailed observations and numerical calculations. Observational studies of star-forming infall are indispensable for understanding the kinematics of gravitational collapse onto young stellar objects (YSOs). This, in turn, is essential for studying the origin of the initial mass function and of multiple systems. Observations are now beginning to probe a variety of size scales, density, and temperature regimes in many sources.

In recent years, millimeter-wavelength observations have increased the evidence for infall motions onto nearby YSOs. The main procedure is to observe spectral lines that trace high densities ($n > 10^4$ cm$^{-3}$) and have redshifted self-absorption spatially concentrated around an embedded YSO. The spatial concentration and the use of dense gas tracers are important to ensure that the observed kinematic signature is associated with the YSO. For instance, Zhou et al. (1993) mapped the globule B335 in the $2_{12}$–$1_{11}$ and $3_{12}$–$2_{11}$ optically thick lines of $H_2CO$ and in the optically thin lines of $C_{18}O$ (1–0) and $C^{34}S$ (2–1). They reproduced the line profiles on spatial scales of 0.02 pc from the source with an inside-out collapse model (Shu 1977). Choi et al. (1995) modeled the same B335 observations with a Monte Carlo radiative transfer code (Bernes 1979), confirming the numerical results from Zhou et al. (1993). Later, Zhou (1995) modeled the observed $H_2CO$ and CS line profiles toward IRAS 16293−2422 as arising from a combination of infall and rotation, using the Terebey, Shu, & Cassen (1984) collapse model. The case for infall motions in these sources is strong because of the detailed observations and modeling that has been done on them. However, in such a small sample of candidates, peculiarities of source structure and kinematics (e.g., outflows or rotation) could possibly account for the apparent signatures of infall. Therefore, these well-studied cases are not sufficient by themselves to support a claim for observed infall motions onto a wide class of sources.

Another approach to searching for infall evidence is to observe a statistically large sample of sources in two lines tracing high-density gas, one optically thick and the other optically thin. In such a sample, rotation and bipolar outflow motions having symmetry axes in random orientations would tend to produce optically thick line profiles with equal numbers of redshifted and blueshifted self-absorption. On the other hand, infall motions in centrally concentrated regions would only produce redshifted self-absorption in the line profiles (Leung & Brown 1977). A spectral line survey of a large source sample should reveal whether there is a statistically significant excess of sources with redshifted or blueshifted self-absorption. This approach does not depend much on the details of the models, but mainly on whether there is a prevalence of inward or outward motions. At the same time, such a study can yield a list of collapse candidates for further detailed studies. Recent surveys aimed at finding candidate collaps-

[1] Hubble Fellow.

ing YSOs include those by Mardones et al. (1994), which used the $C_3H_2$ ($2_{12}$–$1_{01}$) line, Wang et al. (1995), who observed the $H_2CO$ ($3_{12}$–$2_{11}$) line in a sample of Bok globules, and Gregersen et al. (1997), which used $HCO^+$ (4–3) and (3–2) lines in a sample of class 0 sources (Andre, Ward-Thompson, & Barsony 1993). None of these surveys have emphasized the statistical properties of the samples because of the limited number of targets observed.

In this paper, we present the results of a molecular line survey toward 47 of the reddest nearby YSOs, more than twice the number of sources in any of the previous surveys. In § 2, we discuss our source selection criteria, the molecular lines, and the telescopes we used. In § 3, we describe the normalized velocity difference ($\delta V$) between the peaks of optically thick and thin lines, as a quantitative measure of the line profiles. We then analyze statistically the distribution of $\delta V$ for different molecular lines and source subsamples. In § 4, we interpret the statistics kinematically. Finally, we summarize our conclusions in § 5.

## 2. OBSERVATIONS

### 2.1. *Source Sample*

The sources were selected based solely on their observed spectral energy distribution (SED) and estimated distance from the Sun in order to be unbiased with respect to prior knowledge of their molecular line shapes. To select the youngest sources (best infall candidates), we used the bolometric temperature ($T_{bol}$; Myers & Ladd 1993) whenever known; otherwise, we estimated $T_{bol}$ based on *IRAS* and submillimeter continuum observations. $T_{bol}$ is defined as the temperature of a blackbody with the same mean frequency as the source spectrum. Chen et al. (1995) found that class 0 sources have $T_{bol} < 70$ K, and class I sources (Lada & Wilking 1984) have $70 \leq T_{bol} < 650$ K. We imposed a limit of $T_{bol} < 200$ K to select the most embedded class I and class 0 sources. We relied mostly on the papers by Ladd, Lada, & Myers (1993) in Perseus and Chen et al. (1995, 1997) in the Taurus, Ophiuchus, Chamaeleon, Lupus, and Corona Australis star-forming clouds for the determination of $T_{bol}$. Chen et al. required the source fluxes to be known in at least six different wavelengths in order to compute accurate values of $T_{bol}$. That condition is easily met by most *IRAS* sources that also have been detected at optical or near-infrared wavelengths. However, many of the most embedded class I sources and most class 0 sources do not satisfy that requirement. Only a handful of class 0 sources have been observed in enough different millimeter and submillimeter wavelengths to make a good determination of $T_{bol}$ possible (e.g., B335 and L1527; Ladd et al. 1991). We therefore added sources to our list based on more relaxed criteria in order to have a larger sample of the youngest known nearby YSOs.

We required *IRAS* point sources in our sample to have rising spectra between 25 and 100 $\mu$m (with flux ratios 2–4 for wavelength pairs of 25/12, 60/25, and 100/60 $\mu$m) and to be located close to the centers of their parent molecular cloud core maps. These conditions are necessary to exclude Galactic cirrus and extragalactic objects that may have high 100/60 $\mu$m flux ratios. We also added sources with known bright millimeter or submillimeter continuum emission, and nearby class 0 sources known to us by mid-1995. We consulted Casali, Eiroa, & Duncan (1993) for submillimeter continuum observations in Serpens, and Henning et al. (1993) and Reipurth et al. (1993) for submillimeter continuum observations toward southern pre–main-sequence (PMS) stars. We also consulted Persi et al. (1990), Carballo, Wesselius, & Whittet (1992), and Bourke, Hyland, & Robinson (1995) for *IRAS* and near-infrared observations of southern PMS stars, many of them located in Bok globules. We determined $T_{bol}$ for all the sources detected in at least three different wavelengths in order to include sources not quoted in Chen et al. (1995, 1997). The derived values of $T_{bol}$ for sources with poor wavelength coverage are upper limits if they lack long-wavelength fluxes and lower limits if they lack short-wavelength fluxes. Because of our selection criteria, we are confident that $T_{bol} < 200$ K in all sources in our sample. To determine a representative systematic error in $T_{bol}$ in sources with poor short-wavelength spectral coverage, we determined $T_{bol}$ by including and excluding wavelengths shorter than 60 $\mu$m in sources with good spectral coverage. We found that the error in $T_{bol}$ when neglecting wavelengths shorter than 60 $\mu$m is typically less than 20 K for sources having $T_{bol} < 100$ K. Our determination of $T_{bol}$ is consistent with the values given by Gregersen et al. (1997) that are also with limited wavelength coverage.

Table 1 lists all the sources detected in at least one optically thin and one optically thick line. Columns (1) and (2) identify the source, columns (3) and (4) list the observed coordinates (B1950.0), column (5) lists the distance from the Sun in units of parsecs, column (6) lists $T_{bol}$, and column (7) lists the number $N_\lambda$ of continuum fluxes used to derive $T_{bol}$. We give lower or upper limits to $T_{bol}$ rather than values for the sources IRAS 03282+3035, HH 211mm, VLA 1623, and S68N because of the lack of wavelength coverage close to the peak of their SEDs. Although these estimates are crude, they are sufficient for our analysis in § 3, since we only need to know whether or not $T_{bol}$ is below 70 K. Column (8) lists the references we consulted to determine values of $T_{bol}$. Finally, column (9) indicates whether there is outflow evidence from the source either as high-velocity molecular line wings (CO) or as shock fronts (HH).

Even though we did not use the outflow properties as a source selection criterion, 87% of the sources in Table 1 actually show evidence of driving an outflow. This is expected when selecting the most embedded sources, since they tend to drive strong molecular outflows (Bontemps et al. 1996). YSO outflow models usually require mass infall onto an accretion disk (see references in Bachiller 1996), and so there is reason to expect that most sources in this survey must have infalling envelopes. However, we emphasize that in this paper, we are seeking to examine direct kinematic evidence for infall motions onto the sources.

We did not detect 19 of the sources from our initial target list in either the $H_2CO$ line, the $N_2H^+$ line, or both. Table 2 lists the positions and rms noise (main-beam brightness temperature) of the undetected lines for reference. We detected the $N_2H^+$ line toward the sources IRAS 11436−6017 and GSS 30 IRS 1, but it was too weak for a good velocity and width determination (peak $T_{mb}$ of 0.15 and 0.3 K, respectively). We note that the average $T_{bol}$ of these sources in Table 2 is higher than that of the detected sources listed in Table 1. In fact, sources with $T_{bol} < 50$ K in Table 1 were easily detected in all the observed lines.

### 2.2. *Lines*

It is important to observe both optically thick and optically thin lines in order to distinguish double-peak profiles

TABLE 1

SOURCE LIST

| Source[a] (1) | Name (2) | R.A. (1950.0) (3) | Decl. (1950.0) (4) | Distance (pc) (5) | $T_{bol}$ (K) (6) | $N_\lambda$ (7) | References[b] (8) | Outflow[c] (9) |
|---|---|---|---|---|---|---|---|---|
| 03225+3034..... | L1448 IRS 3 | 3 22 31.5 | 30 34 49 | 350 | 70 | 5 | 1, 2 | CO |
| L1448 mm ..... | | 3 22 34.4 | 30 33 35 | 350 | 56 | 6 | 3 | CO, HH |
| 03235+3004..... | | 3 23 33.0 | 30 04 59 | 350 | 136 | 5 | 1, 2 | ... |
| 03245+3002..... | L1455, RNO 15 | 3 24 34.9 | 30 02 36 | 350 | 71 | 5 | 1, 2 | CO |
| 03256+3055..... | | 3 25 39.2 | 30 55 20 | 350 | 74 | 4 | 4 | ... |
| 03259+3105..... | SSV 13 | 3 25 57.9 | 31 05 50 | 350 | 90 | 6 | 2, 5 | CO, HH |
| NGC 1333-2..... | | 3 25 49.9 | 31 04 16 | 350 | 52 | 9 | 6, 7 | CO, HH |
| NGC 1333-4A..... | | 3 26 04.8 | 31 03 13 | 350 | 34 | 8 | 6, 8 | CO |
| NGC 1333-4B..... | | 3 26 06.5 | 31 02 51 | 350 | 36 | 8 | 6, 8 | CO |
| 03282+3035..... | | 3 28 15.2 | 30 35 14 | 350 | 35[d] | 2 | 1 | CO, HH |
| HH 211 mm..... | | 3 40 48.7 | 31 51 24 | 350 | 30[d] | 0 | 9 | CO, HH |
| 04166+2706..... | B213NW | 4 16 36.0 | 27 06 00 | 140 | 139 | 8 | 10 | CO |
| 04169+2702..... | B213NW | 4 16 54.0 | 27 01 59 | 140 | 170 | 11 | 10 | CO |
| 04287+1801..... | L1551 IRS 5 | 4 28 40.2 | 18 01 42 | 140 | 95 | 19 | 10 | CO, HH |
| 04289+1802..... | L1551NE | 4 28 50.8 | 18 02 11 | 140 | 75 | 8 | 10 | ... |
| 04325+2402..... | L1535 | 4 32 33.5 | 24 02 15 | 140 | 157 | 5 | 11 | CO |
| 04365+2535..... | TMC-1A | 4 36 31.2 | 25 35 56 | 140 | 170 | 11 | 10 | CO |
| 04368+2557..... | L1527 | 4 36 49.3 | 25 57 16 | 140 | 60 | 11 | 10 | CO, HH |
| 11051−7706..... | Ced 110 IRS 4 | 11 05 23.1 | −77 06 14 | 150 | 95 | 9 | 11 | CO, HH |
| 11590−6452..... | Sa 136, BHR 71 | 11 59 03.1 | −64 52 11 | 150 | 56 | 5 | 1, 12 | CO, HH |
| 12553−7651..... | | 12 55 20.3 | −76 51 22 | 150 | 99 | 4 | 11 | ... |
| 13036−7644..... | Sa 160, BHR 86 | 13 03 41.4 | −76 44 03 | 150 | 63 | 5 | 11 | CO |
| 15398−3359..... | B228 | 15 39 50.4 | −33 59 42 | 150 | 61 | 4 | 11 | HH |
| 15420−3408..... | Sz 68 | 15 42 01.3 | −34 08 09 | 150 | 120 | 5 | 1, 5 | HH |
| VLA 1623 ..... | | 16 23 24.9 | −24 17 46 | 160 | 30[d] | 4 | 13 | CO, HH |
| WL 22 ..... | IRS 27, YWL 4 | 16 23 57.3 | −24 28 15 | 160 | 86 | 10 | 10 | ... |
| 16244−2432..... | IRS 44, YLW 16 | 16 24 26.2 | −24 32 53 | 160 | 157 | 10 | 10 | CO |
| 16293−2422..... | | 16 29 20.9 | −24 22 16 | 160 | 43 | 6 | 10 | CO |
| 16316−1540..... | L43, RNO 91 | 16 31 37.7 | −15 40 52 | 160 | 79 | 6 | 1, 14 | CO |
| 16544−1604..... | L146, CB 68 | 16 54 27.2 | −16 04 48 | 160 | 74 | 3 | 1 | CO |
| 18148−0440..... | L483 | 18 14 50.6 | −04 40 49 | 200 | 50 | 8 | 1, 14, 15 | CO, HH |
| Serp S68N ..... | | 18 27 15.2 | 01 14 57 | 310 | 40[d] | 4 | 16, 17 | CO |
| Serp FIRS 1..... | | 18 27 17.4 | 01 13 16 | 310 | 51 | 7 | 16, 17 | CO |
| Serp SMM 5 ..... | | 18 27 18.9 | 01 14 36 | 310 | 59 | 7 | 16, 17 | HH |
| Serp SMM 4 ..... | | 18 27 24.3 | 01 11 11 | 310 | 43 | 6 | 16, 17 | CO |
| Serp SMM 3 ..... | | 18 27 27.3 | 01 11 55 | 310 | 46 | 5 | 16, 17 | CO |
| 18331−0035..... | HH 108/109 IRS | 18 33 07.6 | −00 35 48 | 310 | 54 | 4 | 1, 5 | HH |
| CrA IRAS 32..... | | 18 59 35.8 | −37 11 53 | 130 | 148 | 4 | 11 | ... |
| 19156+1906..... | L723 | 19 15 41.3 | 19 06 47 | 200 | 50 | 4 | 1, 5 | CO, HH |
| 19180+1114..... | L673A | 19 18 04.6 | 11 14 12 | 300 | 55 | 4 | 1, 14 | CO |
| 19345+0727..... | B335, CB 199 | 19 34 35.7 | 07 27 20 | 250 | 37 | 10 | 1, 18 | CO, HH |
| 20353+6742..... | L1152 | 20 35 19.4 | 67 42 30 | 350 | 72 | 3 | 1 | CO |
| 20386+6751..... | L1157 | 20 38 39.6 | 67 51 33 | 350 | 62 | 3 | 1 | CO, HH |
| 21017+6742..... | L1172 | 21 01 44.2 | 67 42 24 | 350 | 72 | 5 | 1, 14 | CO |
| 22343+7501..... | L1251A | 22 34 22.0 | 75 01 32 | 300 | 108 | 7 | 1 | CO, HH |
| 22376+7455..... | L1251B | 22 37 40.8 | 74 55 50 | 300 | 91 | 4 | 1 | CO, HH |
| 23238+7401..... | L1262, CB 244 | 23 23 48.7 | 74 01 08 | 250 | 104 | 7 | 1, 191750 | CO |

NOTE.—Units of right ascension are hours, minutes, and seconds, and units of declination are degrees, arcminutes, and arcseconds.

[a] *IRAS* name whenever applicable.

[b] References to SED observations (or $T_{bol}$) only.

[c] CO indicates that an outflow has been detected as high-velocity molecular gas (White et al. 1995; Wu, Huang, & He 1996; Bontemps et al. 1996; Williams et al. 1997). HH indicates that there is evidence of shocked molecular gas from optical or near-infrared line emission (Bally et al. 1993a; Bally, Lada, & Lane 1993b; Bourke 1994; Reipurth 1994; Dent, Matthews, & Walther 1995; Fuller et al. 1995; Devine, Reipurth, & Bally 1997; Eiroa et al. 1997).

[d] Educated guess; we estimate limits $T_{bol} < 50$ K (03282+3035), $T_{bol} > 8$ K (HH 211 and VLA 1623) and $T_{bol} < 80$ K (Serp 68N).

REFERENCES.—(1) *IRAS* Point Source Catalog; (2) Ladd et al. 1993; (3) Bachiller, Andre, & Cabrit 1991; (4) Clark 1991; (5) Reipurth et al. 1993; (6) Jennings et al. 1987; (7) Sandell et al. 1994; (8) Sandell et al. 1991; (9) McCaughrean, Rayner, & Zinnecker 1994; (10) Chen et al. 1995; (11) Chen et al. 1997; (12) Bourke et al. 1995; (13) Andre et al. 1993; (14) Ladd et al. 1991; (15) Fuller et al. 1995; (16) Casali et al. 1993; (17) Hurt & Barsony 1996; (18) Chandler et al. 1990; (19) Yun & Clemens 1995.

produced by optical depth effects from those due to two velocity components along the line of sight. The observed molecules should have a high dipole moment in order to be sensitive to the high-density gas in the immediate neighborhood of the YSO and not to the more extended, lower density gas surrounding the parent cores. Also, the molecular species should be abundant in molecular cloud cores but unaffected by peculiar chemistry effects. For example, SiO and $CH_3OH$ are well known for their enhanced abundances by many orders of magnitude in the outflow lobes of some YSOs (e.g., Bachiller 1996), presumably because of the desorption of molecules from grain mantles in shock fronts.

Following these criteria, we chose the CS ($\mu = 1.96$ debye) and $H_2CO$ ($\mu = 2.33$ debye) molecules to carry out the survey observations. $H_2CO$ was our first choice molecule, following the example of Zhou et al. (1993). The abun-

TABLE 2

SOURCES NOT DETECTED IN EITHER THE $H_2CO$ LINE, THE $N_2H^+$ LINE, OR BOTH

| Source[a] | Name | R.A. (1950.0) | Decl. (1950.0) | Distance (pc) | $T_{bol}$ (K) | References[b] | Line(s) | rms Noise[c] (K) | Telescope |
|---|---|---|---|---|---|---|---|---|---|
| 03382+3145 ..... | | 3 38 15.0 | 31 45 11 | 350 | 85 | 1, 2 | $H_2CO$ | 0.15 | IRAM |
| 03385+3149 ..... | | 3 38 30.9 | 31 49 24 | 350 | 110 | 1, 2 | $H_2CO$, $N_2H^+$ | 0.15, 0.10 | IRAM |
| 04108+2803 ..... | L1495 | 4 10 49.3 | 28 03 00 | 140 | 205 | 3 | $H_2CO$, $N_2H^+$ | 0.15, 0.11 | IRAM |
| 04302+2247 ..... | L1536 | 4 30 16.4 | 22 47 04 | 140 | 202 | 3 | $H_2CO$, $N_2H^+$ | 0.13, 0.10 | IRAM |
| 04361+2547 ..... | | 4 36 06.6 | 25 47 00 | 140 | 144 | 3 | $N_2H^+$ | 0.11 | IRAM |
| Cham B35..... | | 11 05 55.0 | −77 06 18 | 150 | 57 | 4 | $N_2H^+$ | 0.04 | SEST |
| Cham C9-2..... | | 11 07 12.2 | −77 27 37 | 150 | 175 | 4 | $N_2H^+$ | 0.05 | SEST |
| Cham IRN ..... | | 11 07 14.1 | −77 27 28 | 150 | 208 | 4 | $H_2CO$, $N_2H^+$ | 0.12, 0.05 | SEST |
| 11306−6311 ..... | DC 294.3−2.0 | 11 30 42.5 | −63 10 45 | 150 | 71 | 4 | $H_2CO$, $N_2H^+$ | 0.12, 0.04 | SEST |
| 11436−6017 ..... | | 11 43 35.2 | −60 17 27 | 150 | 103 | 4 | $N_2H^+$ | 0.05 | SEST |
| 12500−7658 ..... | | 12 50 03.3 | −76 58 39 | 150 | 94 | 4 | $H_2CO$, $N_2H^+$ | 0.10, 0.04 | SEST |
| 12533−7632 ..... | | 12 53 19.3 | −76 32 12 | 150 | 95 | 4 | $H_2CO$, $N_2H^+$ | 0.09, 0.04 | SEST |
| 15215−6056 ..... | DC 320.5−3.6 | 15 21 30.7 | −60 56 19 | 150 | 84 | 1, 5 | $N_2H^+$ | 0.03 | SEST |
| 16017−3936 ..... | | 16 01 42.5 | −39 36 56 | 150 | 99 | 4 | $H_2CO$, $N_2H^+$ | 0.05, 0.04 | SEST |
| GSS 30 IRS 1..... | | 16 23 19.9 | −24 16 18 | 160 | 175 | 3 | $N_2H^+$ | 0.10 | SEST |
| Oph IRS 8 ..... | | 16 22 46.3 | −24 11 43 | 160 | 203 | 3 | $H_2CO$, $N_2H^+$ | 0.15, 0.13 | IRAM |
| 16245−3859 ..... | | 16 24 30.2 | −38 59 07 | 150 | 129 | 4 | $H_2CO$, $N_2H^+$ | 0.04, 0.04 | SEST |
| 17151−3202 ..... | DC 354.2+3.2 | 17 15 08.6 | −32 02 24 | 170 | 134 | 1, 5 | $H_2CO$, $N_2H^+$ | 0.05, 0.04 | SEST |
| 19180+1116 ..... | L673B | 19 18 01.3 | 11 16 27 | 300 | 94 | 1, 6 | $H_2CO$, $N_2H^+$ | 0.17, 0.19 | IRAM |

NOTE.—Units of right ascension are hours, minutes, and seconds, and units of declination are degrees, arcminutes, and arcseconds.

[a] *IRAS* name whenever applicable.

[b] References to SED observations (or $T_{bol}$) only.

[c] Noise in units of $T_{mb}$.

REFERENCES.—(1) *IRAS* Point Source Catalog; (2) Ladd et al. 1993; (3) Chen et al. 1995; (4) Chen et al. 1997; (5) Persi et al. 1990; (6) Ladd et al. 1991.

dance of $H_2CO$ is known to be only moderately enhanced in bipolar outflows (Bachiller & Pérez 1997). We subsequently observed part of the survey in the CS molecule in order to check that our results were not being biased by peculiar chemistry in low-mass star-forming regions. We believe the CS and $H_2CO$ lines are generally optically thick because of the observed brightness temperatures and line shapes. In a few cases, when the line is weak ($T_{mb} \leq 1$ K) and approximately of Gaussian shape, it is likely to be optically thin (e.g., L673A, 04325+2402, and L1172; see Figs. 1 and 2).

Ideally, one would observe an isotope of the optically thick tracer molecule as the optically thin tracer. Then both lines would probe the same density, temperature, and chemistry and would be observed with essentially the same angular resolution. However, in general, the 2 mm $H_2^{13}CO$ and the 3 mm $C^{34}S$ lines are too weak for an accurate determination of line velocities in a large source sample. We chose to observe the $N_2H^+$ $J = 1$–0 line instead ($\mu = 3.4$ debye). This molecule has seven hyperfine components, in two groups of three lines and one isolated component ($JF_1F_2 = 101$–012). Caselli, Myers, & Thaddeus (1995) determined the frequencies of all components with a precision of 6 kHz (0.02 km s$^{-1}$). The hyperfine structure of $N_2H^+$ also permits a determination of the optical depth in the line, thus allowing an internal check on the thinness of the isolated $N_2H^+$(101–012) line. Caselli et al. showed that among the seven components, only two show any evidence of anomalous excitation ($F_1F_2 = 12$–12 and $F_1F_2 =$ 10–11), and that these anomalies represent a departure of less than 20% from the value expected in LTE. Any such small anomaly in hyperfine line ratios is included in the estimated uncertainty of the optical depth. This uncertainty is generally much smaller than the estimated optical depths. Womack, Ziurys, & Wyckoff (1992) found that the $N_2H^+$ $J = 1$–0 line is narrow in dark clouds, with no evidence of line wings. The $N_2H^+$ line widths and hyperfine components make it an ideal probe of the systemic velocity toward young stellar objects.

### 2.3. *Telescopes*

We used the IRAM 30 m telescope in Pico Veleta, Spain, in 1995 May 10–12. We observed simultaneously in the 2 and 3 mm atmospheric windows with receivers tuned to the ortho-$H_2CO$ ($2_{12}$–$1_{11}$) (140.839518 GHz) and $N_2H^+$ (101–012) (93.176265 GHz) lines, respectively. The line rest frequencies were taken from Lovas (1991) and Caselli et al. (1995), respectively. The back end had a digital correlator with spectral resolutions of 20 and 10 kHz at 2 and 3 mm wavelengths, respectively (0.04 and 0.03 km s$^{-1}$). We used overlap frequency switching by $\pm$3.85 MHz because this method is efficient and ensures that the observed line profiles are free of emission from an off-position. We checked pointing regularly with continuum sources and found it good to better than 5″. Typical system temperatures were $\sim$400 K at 2 mm and $\sim$350 K at 3 mm. The main-beam efficiency at 93 and 141 GHz was taken to be 73% and 55%, respectively.

We used the SEST 15 m telescope in La Silla, Chile, in 1995 September 19–20 and 24, to observe simultaneously the same 2 and 3 mm $H_2CO$ and $N_2H^+$ lines as with the IRAM 30 m telescope. The weather was excellent, with system temperatures around 150 K in both lines. We split the high-resolution acousto-optical spectrometer into two bands, providing a spectral resolution of 43 kHz in each band (0.138 km s$^{-1}$ at 93 GHz and 0.11 km s$^{-1}$ at 141 GHz). The acousto-optical spectrometer sometimes produces spurious emission features in the central 3–5 channels; so to avoid interference with the observed spectral lines, we centered the spectrometer off the rest velocity of each source by 2–8 km s$^{-1}$. We also observed a subsample of sources in the para-$H_2CO$ ($2_{02}$–$1_{11}$) transition at 145.602953 GHz and the $C^{34}S$ (2–1) transition at 96.412982 GHz. We used main-beam efficiencies of 74% at 93 and 96

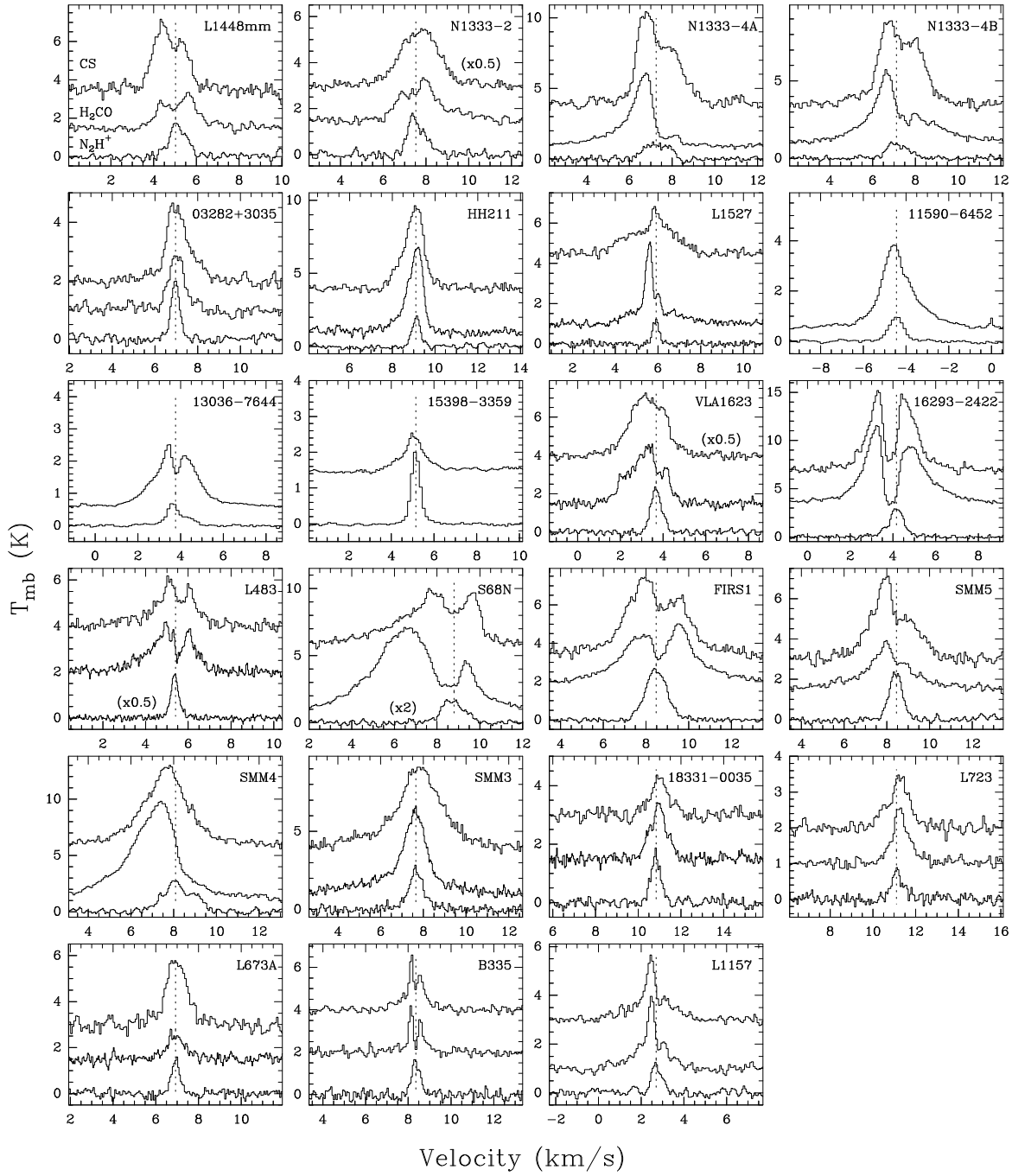


FIG. 1.—Observed spectral line profiles toward the sources with $T_{bol} < 70$ K in our sample (class 0). $N_2H^+$ (101–012) is drawn at the bottom of each box, $H_2CO$ ($2_{12}$–$1_{11}$) is next (*middle*), and CS (2–1) is at the top whenever it was observed. The vertical scale is in main-beam brightness temperature units. The horizontal scale has a range of 10 km $s^{-1}$ in all sources. The dotted line indicates the $N_2H^+$ velocity found with the hyperfine-structure fit (the other six hyperfine components lie off the box).

GHz, 68% at 141 GHz, and 67% at 145 GHz, as indicated in the SEST handbook.

In 1995 December 7–11 and 29–31, we used the NEROC Haystack[2] 37 m telescope to observe the sources visible from Haystack in the CS (2–1) line at 97.980968 GHz. We observed left and right circular polarizations simultaneously with two SIS receivers. The back end had a digital correlator that we used with 17.8 MHz bandwidth and 13 kHz spectral resolution (0.04 km $s^{-1}$). Typical system temperatures were 200 K. The antenna main-beam FWHM at 98 GHz (21″) compares well with the IRAM 2 and 3 mm beams. We measured a main-beam efficiency of $\sim 16\% \pm 3\%$ by scaling spectra of IRC +10216 to those taken at the IRAM 30 m telescope by Mauersberger et al. (1989).

[2] Radio astronomy observations at the NEROC Haystack Observatory of the Northeast Radio Observatory Corporation (NEROC) are supported by a grant from the National Science Foundation.

## 3. RESULTS

### 3.1. *Variety of Observed Spectral Line Profiles*

Figure 1 shows the observed spectra toward all the class 0

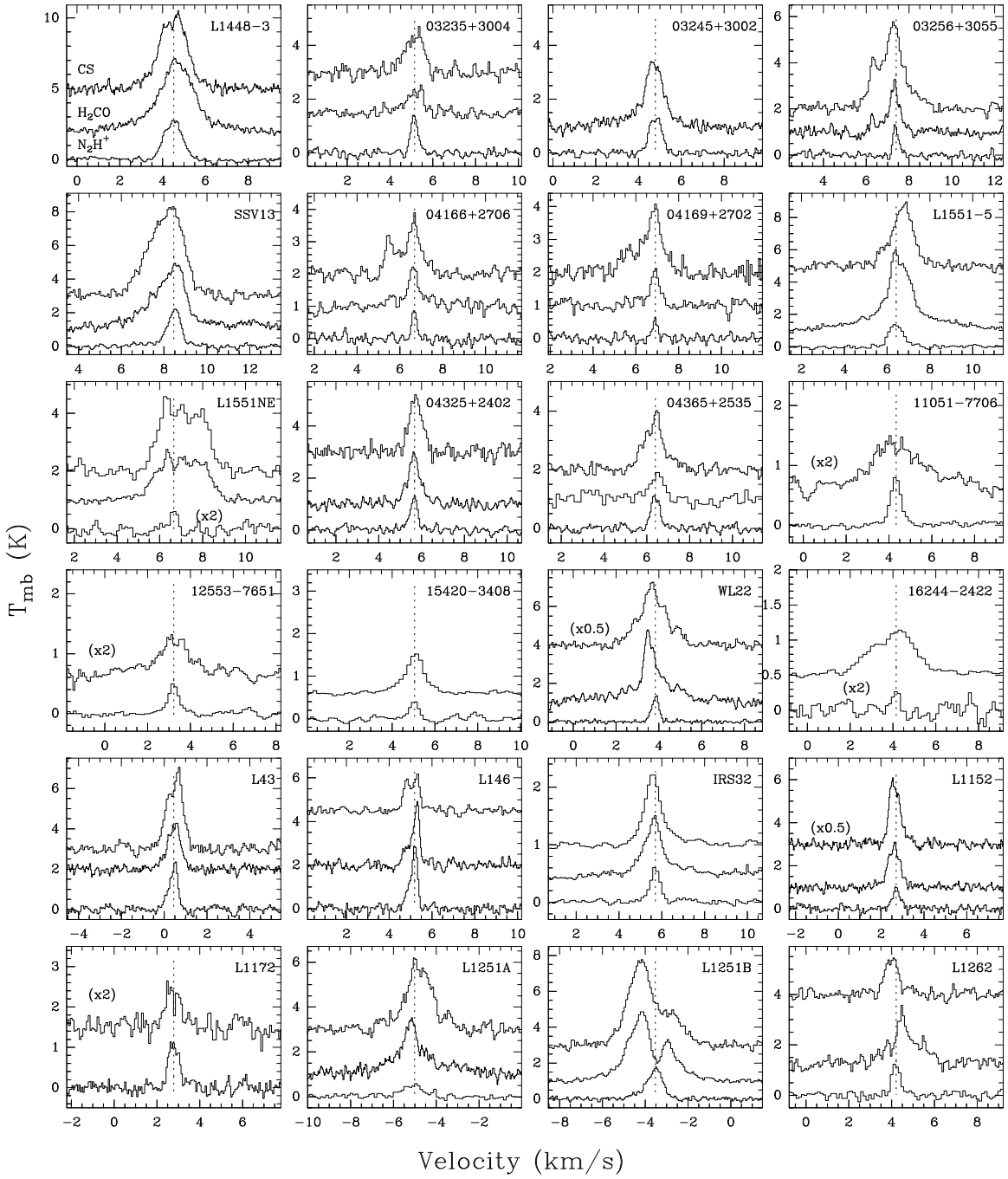


FIG. 2.—Observed spectral line profiles toward the sources with $T_{bol} \geq 70$ K in our sample (class I). The display format is the same as in Fig. 1.

sources ($T_{bol} < 70$ K) in our sample ordered by right ascension, and Figure 2 shows the spectra obtained toward the class I sources ($70 \leq T_{bol} \leq 200$ K). The $N_2H^+$ (101–012) line is drawn at the bottom of each box, $H_2CO$ ($2_{12}$–$1_{11}$) is drawn in the middle, and CS (2–1) is drawn at the top if it was observed. In a few sources, such as IRAS 16244−2422, the $N_2H^+$(101–012) line is very weak, but the velocity (*dotted line*) is sufficiently well determined because it is based on all seven hyperfine components, not just the one shown. We find a wide variety of spectral line profiles in the $H_2CO$ and CS lines in our sample: double peaked, with a peak and a "shoulder," and single symmetric lines. In addition, many sources have high-velocity wings associated with unbound motions (outflows).

The CS and $H_2CO$ line shapes differ from source to source but are usually similar to each other. The $N_2H^+$ line, on the other hand, is Gaussian toward almost all sources. In sources with symmetric $H_2CO$ and CS lines, their peak velocity lies very close to that of the $N_2H^+$ line. In sources with double-peaked $H_2CO$ and CS lines, the $N_2H^+$ peak velocity lies between the two peaks (or between the peak and the shoulder), indicating that the complex $H_2CO$ and CS line profiles arise from self-absorption at low velocities. As proof of the lower optical depth of $N_2H^+$, we derive optical depths $\tau < 1$ in the 101–012 line in 93% of the sources, and $\tau < 1.6$ in all of them.

In most class I sources, the $H_2CO$ and CS lines are broader than the $N_2H^+$ line, but all three line profiles are essentially symmetric, showing no evidence of self-absorption (Fig. 2). On the other hand, many of the observed CS and $H_2CO$ profiles toward the class 0 sources show evidence of self-absorption. The $H_2CO$ and/or CS spectral profiles are asymmetric with respect to the $N_2H^+$ center velocity in 15 out of 23 class 0 sources (Fig. 1). Most of these asymmetric profiles have peaks whose velocity is significantly blueshifted, rather than redshifted, from the velocity of the optically thin $N_2H^+$ line. This high incidence of self-absorption toward class 0 sources is similar to what Gregersen et al. (1997) found in $HCO^+$ lines.

Besides the variation in line shapes discussed above, the line widths vary by a factor of 5 over our source sample. For example, the FWHM of the $N_2H^+$ line varies from 0.3 km $s^{-1}$ in Taurus to 1.8 km $s^{-1}$ in Serpens. This is important to bear in mind when we use the peak velocity shift between lines to compare different sources in the following section.

### 3.2. *Quantifying Spectral Line Asymmetries*

To study the distribution of line profiles statistically, we need to quantify the observed line asymmetries. To do this, we define the nondimensional parameter

$$\delta V = (V_{\rm thick} - V_{\rm thin})/\Delta V_{\rm thin}\,, \quad (1)$$

the velocity difference between the peaks of the optically thick and thin lines, normalized by the FWHM of the thin line. We use the normalized velocity difference $\delta V$ rather than the velocity difference $V_{\rm thin} - V_{\rm thick}$ to reduce bias arising from lines having different widths from one source to the next. This is a significant effect in our sample, as discussed above, and the normalization ensures that two lines of the same shape will have the same measure of asymmetry even if they have significantly different widths. To compute $\delta V$, we first fitted a Gaussian to the brightest peak of the optically thick line in order to define its velocity ($V_{\rm thick}$). We then fitted seven Gaussian hyperfine components to the $N_2H^+$ $J = 1$–0 line using the line parameters derived by Caselli et al. (1995); this gives the $N_2H^+$ velocity and FWHM ($V_{\rm thin}$ and $\Delta V_{\rm thin}$).

We believe that $\delta V$ is a more convenient and robust measure of the line asymmetry than the even-odd component decomposition (Mardones et al. 1994), the shift in line centroid (Adelson & Leung 1988; Walker, Narayanan, & Boss 1994), the ratio of blue to red peak brightness (Myers et al. 1995), and the line skewness (Gregersen et al. 1997). The even-odd decomposition is too sensitive to the choice of reference velocity, and the line centroid is too sensitive to the choice of velocity window. The ratio of blue to red peak brightness cannot be used for lines where a second peak is not well defined. The skewness is much more sensitive than is $\delta V$ to asymmetry in the line wings, which may be due to outflow, not infall motions. On the other hand, the adopted $\delta V$ has the disadvantage that it is ambiguous for double-peaked lines with nearly equal peak intensities. In our sample, this occurs in only three sources in the CS line (IRAS 16293−2422, L483, and Serp S68N) and one source in the $H_2CO$ line (L483; see Fig. 1). In the CS spectra, the ratio of the blue-red temperature difference to the rms noise $[(T_b - T_r)/\sigma]$ is 3.7, 3.0, and 0.8 in the sources IRAS 16293−2422, L483, and Serp S68N, respectively, and in the L483 $H_2CO$ spectrum, the same ratio is 2.4. We regard a ratio of 2.0 or less as insignificant, and so we drop the CS line in Serp S68N from the sample.

We investigated alternatives to fitting Gaussians to obtain the velocity of peak emission for the optically thick $H_2CO$ and CS lines. We explored measuring the velocity of the peaks directly from the spectra, calculating the moments of the spectra, and finding the velocity of the peak of the cross correlation of the optically thick and thin line profiles. For simple lines, all methods agree to within the rms uncertainty in center velocity because of rms noise. We adopt the direct-fit method because it appears slightly more robust than the cross-correlation or first-moment methods for sources with significant wing emission. In the optically thin $N_2H^+$ $J = 1$–0 line, the results of fitting seven Gaussian hyperfine components and of fitting a single Gaussian to the isolated 101–012 line are consistent to within 0.01 km $s^{-1}$, but the error in the former is smaller.

Table 3 lists our main survey data: the observed velocities in the ortho-$H_2CO$ ($2_{12}$–$1_{11}$), CS (2–1), and $N_2H^+$(1–0) lines and the values of $\delta V_{\rm H_2CO} = (V_{\rm H_2CO} - V_{\rm N_2H^+})/\Delta V_{\rm N_2H^+}$ and $\delta V_{\rm CS} = (V_{\rm CS} - V_{\rm N_2H^+})/\Delta V_{\rm N_2H^+}$ computed from these velocities, as in equation (1). Table 4 lists the observed velocities in the smaller sample of para-$H_2CO$ ($2_{02}$–$1_{01}$) and $C^{34}S$ (2–1) lines, which we observed as consistency checks. The velocity error estimates from the fitting routines are usually smaller than the channel width (except in low signal-to-noise ratio spectra). We quote either one-half the channel width or the Gaussian estimate as the error in our peak velocity determinations, whichever is bigger. The error in $V_{\rm thin} - V_{\rm thick}$ is usually dominated by the error in the optically thick line profile velocity. This error is typically $\sim$0.03 km $s^{-1}$ and is always smaller than 0.11 km $s^{-1}$.

### 3.3. *Distributions of Normalized Velocity Differences*

Figure 3 shows histograms of the distribution of $\delta V_{\rm H_2CO}$ and $\delta V_{\rm CS}$. The IRAM observations were used in Figure 3 whenever sources were observed with both the SEST and IRAM telescopes because of the better spectral and spatial resolution (i.e., each source is counted once). The histograms are clearly skewed toward negative velocities. This also can be seen from the means and standard errors of the mean of the distributions $\langle \delta V_{\rm H_2CO} \rangle = -0.15 \pm 0.08$ and $\langle \delta V_{\rm CS} \rangle = -0.16 \pm 0.07$ given in Table 5. We now explore the statistical significance of this result.

We use the Student's $t$-test for a sample with unknown spread, in order to compare the $\delta V$ distributions with a zero mean normal distribution (our null hypothesis), and derive the probability ($p$) of the null hypothesis. The probability of drawing the distribution of $\delta V$ from a zero mean normal parent distribution is only 5% (3%) for the $H_2CO$ (CS) sample.

Another way to quantify the asymmetries in the distribution of $\delta V$ is to simply count the excess ($E$) number of sources with negative compared with positive $\delta V$. We define the "blue excess" $E$ as $(N_- - N_+)/N$, where $N_-$ is the number of sources with a "significant" blueshift ($\delta V < -0.25$), $N_+$ is the number of sources with a "significant" redshift ($\delta V > 0.25$), $N_0$ is the number of sources with no significant shift ($-0.25 \le \delta V \le 0.25$), and $N$ is the total number of sources. Defined in this way, a large excess ($E$) corresponds to a small probability ($p$). We chose the threshold value 0.25 in the definition of $E$ at about 5 times the typical rms error in $\delta V$ (Table 3) in order to screen out random contributions. The excess of sources with nega-

TABLE 3

$H_2CO$ ($2_{12}$–$1_{11}$), CS (2–1), AND $N_2H^+$ (1–0) SPECTRAL LINE VELOCITIES

| Source | Telescope[a] | $V_{H_2CO}$ (km s$^{-1}$) | $V_{CS}$ (km s$^{-1}$) | $V_{N_2H^+}$ (km s$^{-1}$) | $\Delta V_{N_2H^+}$ (km s$^{-1}$) | $\delta V_{H_2CO}$ | $\delta V_{CS}$ |
|---|---|---|---|---|---|---|---|
| L1448 IRS 3..... | IRAM | 4.68 ± 0.02[b] | 4.70 ± 0.02 | 4.52 ± 0.01 | 0.96 ± 0.01 | 0.16 ± 0.02 | 0.19 ± 0.02 |
| L1448 mm ..... | IRAM | 5.59 ± 0.03 | 4.39 ± 0.02 | 5.02 ± 0.02 | 0.84 ± 0.05 | 0.67 ± 0.06 | −0.75 ± 0.06 |
| 03235+3004..... | IRAM | 5.18 ± 0.02 | 5.19 ± 0.03 | 5.14 ± 0.01 | 0.35 ± 0.01 | 0.11 ± 0.06 | 0.15 ± 0.09 |
| L1455 ..... | IRAM | 4.72 ± 0.02 | ... | 4.78 ± 0.01 | 0.69 ± 0.01 | −0.09 ± 0.03 | ... |
| 03256+3055..... | IRAM | 7.32 ± 0.02 | 7.28 ± 0.02 | 7.39 ± 0.01 | 0.34 ± 0.01 | −0.21 ± 0.07 | −0.31 ± 0.07 |
| SSV 13 ..... | IRAM | 8.55 ± 0.02 | 8.36 ± 0.03 | 8.45 ± 0.01 | 0.72 ± 0.01 | 0.14 ± 0.03 | −0.13 ± 0.04 |
| NGC 1333-2..... | IRAM | 7.98 ± 0.03 | 7.71 ± 0.02 | 7.52 ± 0.01 | 0.94 ± 0.01 | 0.49 ± 0.03 | 0.20 ± 0.02 |
| NGC 1333-4A..... | IRAM | 6.63 ± 0.02 | 6.73 ± 0.02 | 7.25 ± 0.01 | 1.32 ± 0.02 | −0.47 ± 0.02 | −0.39 ± 0.02 |
| NGC 1333-4B..... | IRAM | 6.60 ± 0.02 | 6.75 ± 0.03 | 7.11 ± 0.01 | 1.04 ± 0.02 | −0.49 ± 0.02 | −0.34 ± 0.03 |
| 03282+3035..... | IRAM | 7.02 ± 0.02 | 6.99 ± 0.02 | 6.96 ± 0.01 | 0.47 ± 0.03 | 0.13 ± 0.05 | 0.06 ± 0.05 |
| HH 211 mm..... | IRAM | 9.16 ± 0.02 | 9.07 ± 0.02 | 9.10 ± 0.01 | 0.45 ± 0.02 | 0.13 ± 0.05 | −0.06 ± 0.05 |
| 04166+2706..... | IRAM | 6.62 ± 0.02 | 6.65 ± 0.02 | 6.68 ± 0.01 | 0.34 ± 0.01 | −0.16 ± 0.07 | −0.08 ± 0.07 |
| 04169+2702..... | IRAM | 6.90 ± 0.02 | 6.88 ± 0.02 | 6.91 ± 0.01 | 0.29 ± 0.01 | 0.03 ± 0.08 | −0.11 ± 0.08 |
| L1551 IRS 5..... | IRAM | 6.39 ± 0.02 | 6.77 ± 0.02 | 6.42 ± 0.01 | 0.80 ± 0.01 | −0.04 ± 0.03 | 0.44 ± 0.03 |
| L1551NE ..... | IRAM | 7.02 ± 0.02 | 7.05 ± 0.02 | 6.65 ± 0.01 | 0.47 ± 0.03 | 0.78 ± 0.07 | 0.85 ± 0.07 |
| 04325+2402..... | IRAM | 5.65 ± 0.02 | 5.73 ± 0.02 | 5.67 ± 0.01 | 0.40 ± 0.01 | −0.06 ± 0.06 | 0.14 ± 0.06 |
| 04365+2535..... | IRAM | 6.45 ± 0.04 | 6.46 ± 0.02 | 6.40 ± 0.01 | 0.42 ± 0.01 | 0.11 ± 0.05 | 0.14 ± 0.05 |
| L1527 ..... | IRAM | 5.59 ± 0.02 | 5.91 ± 0.02 | 5.91 ± 0.01 | 0.32 ± 0.01 | −0.99 ± 0.08 | 0.01 ± 0.07 |
| 11051−7706..... | SEST | 4.20 ± 0.11 | ... | 4.33 ± 0.01 | 0.63 ± 0.01 | −0.20 ± 0.18 | ... |
| 11590−6452..... | SEST | −4.59 ± 0.02 | ... | −4.46 ± 0.01 | 0.88 ± 0.03 | −0.15 ± 0.03 | ... |
| 12553−7651..... | SEST | 3.24 ± 0.05 | ... | 3.22 ± 0.01 | 0.46 ± 0.01 | 0.05 ± 0.11 | ... |
| 13036−7644..... | SEST | 3.36 ± 0.03 | ... | 3.76 ± 0.01 | 1.01 ± 0.02 | −0.40 ± 0.03 | ... |
| 15398−3359..... | SEST | 5.05 ± 0.02 | ... | 5.14 ± 0.01 | 0.49 ± 0.01 | −0.17 ± 0.05 | ... |
| 15420−3408..... | SEST | 5.09 ± 0.02 | ... | 5.04 ± 0.01 | 0.58 ± 0.03 | 0.10 ± 0.04 | ... |
| VLA 1623 ..... | IRAM | 3.31 ± 0.02 | 3.27 ± 0.02 | 3.67 ± 0.01 | 0.56 ± 0.01 | −0.64 ± 0.04 | −0.71 ± 0.04 |
| | SEST | 3.15 ± 0.02 | ... | 3.65 ± 0.01 | 0.71 ± 0.01 | ... | ... |
| WL 22 ..... | IRAM | 3.50 ± 0.02 | 3.66 ± 0.02 | 3.83 ± 0.01 | 0.33 ± 0.01 | −0.99 ± 0.07 | −0.53 ± 0.07 |
| | SEST | 3.59 ± 0.02 | ... | 3.80 ± 0.01 | 0.53 ± 0.01 | ... | ... |
| 16244−2432..... | SEST | 4.28 ± 0.02 | ... | 4.14 ± 0.01 | 0.72 ± 0.05 | 0.19 ± 0.03 | ... |
| | IRAM | 3.12 ± 0.02 | 3.25 ± 0.02 | 4.16 ± 0.01 | 0.78 ± 0.01 | −1.34 ± 0.03 | −1.16 ± 0.03 |
| 16293−2422..... | SEST | 3.09 ± 0.02 | ... | 4.04 ± 0.01 | 1.13 ± 0.02 | ... | ... |
| L43 ..... | IRAM | 0.46 ± 0.02 | 0.64 ± 0.02 | 0.44 ± 0.01 | 0.48 ± 0.01 | 0.04 ± 0.05 | 0.40 ± 0.05 |
| | SEST | 0.44 ± 0.02 | ... | 0.49 ± 0.01 | 0.60 ± 0.01 | ... | ... |
| L146..... | IRAM | 5.28 ± 0.02 | 5.28 ± 0.02 | 5.18 ± 0.01 | 0.39 ± 0.01 | 0.25 ± 0.06 | 0.25 ± 0.06 |
| | SEST | 5.22 ± 0.02 | ... | 5.15 ± 0.01 | 0.56 ± 0.01 | ... | ... |
| L483..... | IRAM | 4.95 ± 0.02 | 5.13 ± 0.02 | 5.40 ± 0.01 | 0.47 ± 0.01 | −0.95 ± 0.05 | −0.59 ± 0.05 |
| | SEST | 5.12 ± 0.03 | ... | 5.40 ± 0.01 | 0.58 ± 0.01 | ... | ... |
| Serp S68N ..... | IRAM | 6.67 ± 0.02 | 7.83 ± 0.02 | 8.79 ± 0.01 | 1.32 ± 0.04 | −1.61 ± 0.05 | −0.73 ± 0.03 |
| Serp FIRS 1..... | IRAM | 9.64 ± 0.02 | 7.92 ± 0.04 | 8.47 ± 0.01 | 1.11 ± 0.01 | 1.05 ± 0.02 | −0.50 ± 0.04 |
| | SEST | 7.91 ± 0.04 | ... | 8.40 ± 0.01 | 1.29 ± 0.01 | ... | ... |
| Serp SMM 5 ..... | IRAM | 7.93 ± 0.02 | 7.84 ± 0.02 | 8.44 ± 0.01 | 0.69 ± 0.01 | −0.74 ± 0.03 | −0.87 ± 0.03 |
| | SEST | 7.85 ± 0.02 | ... | 8.42 ± 0.01 | 0.99 ± 0.01 | ... | ... |
| Serp SMM 4 ..... | IRAM | 7.35 ± 0.02 | 7.69 ± 0.02 | 8.08 ± 0.01 | 1.84 ± 0.03 | −0.40 ± 0.01 | −0.21 ± 0.01 |
| | SEST | 7.59 ± 0.02 | ... | 8.12 ± 0.01 | 1.80 ± 0.02 | ... | ... |
| Serp SMM 3 ..... | IRAM | 7.60 ± 0.02 | 7.80 ± 0.02 | 7.64 ± 0.01 | 0.82 ± 0.01 | −0.05 ± 0.03 | 0.19 ± 0.03 |
| 18331−0035..... | IRAM | 10.97 ± 0.02 | 10.99 ± 0.02 | 10.83 ± 0.01 | 0.59 ± 0.01 | 0.22 ± 0.04 | 0.25 ± 0.04 |
| | SEST | 10.92 ± 0.02 | ... | 10.84 ± 0.01 | 0.71 ± 0.02 | ... | ... |
| CrA IRAS 32..... | SEST | 5.66 ± 0.02 | 5.58 ± 0.02 | 5.70 ± 0.01 | 0.52 ± 0.01 | −0.07 ± 0.04 | −0.22 ± 0.04 |
| L723..... | IRAM | 11.25 ± 0.02 | 11.27 ± 0.02 | 11.14 ± 0.01 | 0.63 ± 0.02 | 0.17 ± 0.04 | 0.21 ± 0.04 |
| L673A..... | IRAM | 6.94 ± 0.02 | 6.97 ± 0.02 | 6.92 ± 0.01 | 0.47 ± 0.01 | 0.03 ± 0.05 | 0.11 ± 0.05 |
| B335..... | IRAM | 8.13 ± 0.02 | 8.14 ± 0.02 | 8.35 ± 0.01 | 0.48 ± 0.01 | −0.46 ± 0.05 | −0.43 ± 0.05 |
| | SEST | 8.12 ± 0.02 | ... | 8.35 ± 0.01 | 0.53 ± 0.01 | ... | ... |
| L1152 ..... | IRAM | 2.60 ± 0.02 | 2.63 ± 0.02 | 2.70 ± 0.01 | 0.40 ± 0.01 | −0.24 ± 0.06 | −0.19 ± 0.06 |
| L1157 ..... | IRAM | 2.46 ± 0.02 | 2.43 ± 0.02 | 2.69 ± 0.01 | 0.71 ± 0.01 | −0.33 ± 0.03 | −0.36 ± 0.03 |
| L1172 ..... | IRAM | 2.73 ± 0.04 | ... | 2.78 ± 0.01 | 0.53 ± 0.01 | −0.10 ± 0.08 | ... |
| L1251A ..... | IRAM | −5.21 ± 0.02 | −4.80 ± 0.03 | −5.02 ± 0.02 | 0.69 ± 0.09 | −0.28 ± 0.05 | 0.31 ± 0.07 |
| L1251B ..... | IRAM | −4.26 ± 0.02 | −4.22 ± 0.02 | −3.53 ± 0.01 | 1.00 ± 0.01 | −0.73 ± 0.02 | −0.69 ± 0.02 |
| L1262 ..... | IRAM | 4.49 ± 0.02 | 4.00 ± 0.02 | 4.21 ± 0.01 | 0.45 ± 0.01 | 0.62 ± 0.05 | −0.46 ± 0.05 |

[a] The CS spectra were obtained at the Haystack Observatory, with the exception of CrA IRAS 32, which was obtained at the SEST.
[b] The error we quote is the larger of one-half the channel width and the formal 1 $\sigma$ error from a Gaussian fit to the line peak.

tive $\delta V$ in the histograms in Figure 3 is 21% and 29% for the $H_2CO$ and CS samples, respectively (25% overall).

To understand the origin of the asymmetry of the $\delta V$ distribution, we evaluate statistics for subsamples defined by whether $T_{bol}$ corresponds to a class 0 or a class I source (from here on, we refer to sources with $T_{bol} < 70$ K as class 0 and to sources with $70 \leq T_{bol} \leq 200$ K as class I). Table 5 lists (for the full sample and these subsamples) the quantities $N$, $N_-$, $N_0$, and $N_+$, the mean, $p$, and $E$ for the distributions of $\delta V_{H_2CO}$ and $\delta V_{CS}$.

Table 5 shows that the sample sources with $T_{bol} < 70$ K are *entirely* responsible for the histogram skewness in Figure 3. Thus, class 0 sources have a probability of being drawn from a zero mean normal distribution of 4% (0.4%)

TABLE 4

$H_2CO$ ($2_{02}$–$1_{01}$) AND $C^{34}S$ (2–1) SPECTRAL LINE VELOCITIES

| Source | Telescope | $V_{H_2CO}$ (km s$^{-1}$) | $V_{C^{34}S}$ (km s$^{-1}$) | $\Delta V_{C^{34}S}$ (km s$^{-1}$) |
|---|---|---|---|---|
| L1527..... | IRAM | ... | 5.94 ± 0.02 | 0.30 ± 0.05 |
| 13036−7644 ..... | SEST | 3.42 ± 0.02 | 3.72 ± 0.04 | 0.53 ± 0.10 |
| VLA 1623 ..... | SEST | 3.54 ± 0.02 | 3.58 ± 0.05 | 1.37 ± 0.12 |
| WL 22..... | SEST | 3.58 ± 0.02 | 3.87 ± 0.02 | 0.74 ± 0.04 |
| 16293−2422 ..... | SEST | 3.22 ± 0.02 | 4.02 ± 0.06 | 1.78 ± 0.21 |
| L483 ..... | SEST | 5.31 ± 0.05 | 5.40 ± 0.02 | 0.71 ± 0.05 |
| Serp FIRS 1 ..... | SEST | 7.96 ± 0.02 | 8.53 ± 0.03 | 1.32 ± 0.08 |
| Serp SMM 5..... | SEST | 7.87 ± 0.07 | 8.40 ± 0.03 | 0.97 ± 0.09 |
| Serp SMM 4..... | SEST | 7.55 ± 0.02 | 8.11 ± 0.05 | 2.07 ± 0.21 |
| 18331−0035 ..... | SEST | 10.82 ± 0.02 | 10.86 ± 0.03 | 0.37 ± 0.07 |
| CrA IRS 32 ..... | SEST | 5.69 ± 0.02 | 5.72 ± 0.05 | 0.72 ± 0.11 |
| B335 ..... | SEST | 8.16 ± 0.02 | 8.43 ± 0.04 | 0.59 ± 0.10 |
| L1251B..... | IRAM | ... | −3.74 ± 0.05 | 1.42 ± 0.12 |

for the $H_2CO$ (CS) sample, while class I sources have a probability of 81% (99%) for the $H_2CO$ (CS) sample. The overall excess of 25% of sources with negative $\delta V$ can be decomposed in a 47% excess (39% for $H_2CO$ and 55% for CS) among the class 0 sources, and 2% excess (4% and 0%, respectively) among the class I sources. This is illustrated in Figure 4, which shows the $\delta V$ distributions as a function of $T_{bol}$ for the $H_2CO$ and CS lines. The fraction of blueshifted sources (negative $\delta V$) in Figure 4 is clearly greater for class 0 than for class I sources.

To summarize, sources with $T_{bol} < 200$ K (class 0 and class I) tend to have asymmetric profiles in both of the optically thick lines that we used to trace high densities ($> 10^4$ cm$^{-3}$). In this sample, there are ~25% more sources with a significant blueshift than with a significant redshift. This statistically significant tendency arises entirely from

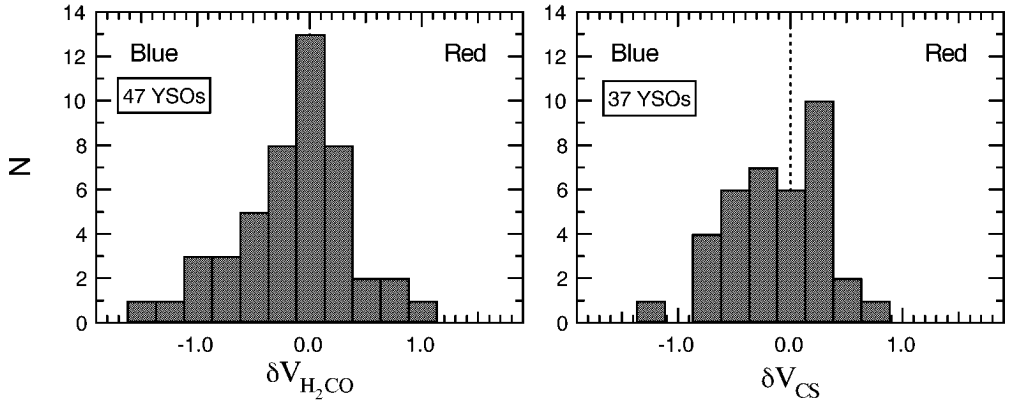


FIG. 3.—The distribution of the line peak velocity difference $\delta V$, defined in eq. (1), for the full sample using $H_2CO$ (*left*) and CS (*right*) as the optically thick line tracer. Note that more sources have negative (blue) than positive (red) values of $\delta V$.

TABLE 5

STATISTICAL PROPERTIES OF THE DISTRIBUTIONS OF $\delta V$

| Optically Thick Line | Sample | $N$ | $N_-$[a] | $N_0$[a] | $N_+$[a] | mean ± s.e.m. | $p$[b] | $E$[c] |
|---|---|---|---|---|---|---|---|---|
| $H_2CO$ ..... | All | 47 | 15 | 27 | 5 | −0.14 ± 0.08 | 0.06 | 0.21 |
| | $T_{bol} \leq 70$ K | 23 | 12 | 8 | 3 | −0.28 ± 0.13 | 0.05 | 0.39 |
| | $70 < T_{bol} < 200$ K | 24 | 3 | 19 | 2 | −0.02 ± 0.07 | 0.81 | 0.04 |
| CS ..... | All | 37 | 14 | 19 | 4 | −0.14 ± 0.07 | 0.04 | 0.27 |
| | $T_{bol} \leq 70$ K | 19 | 10 | 9 | 0 | −0.28 ± 0.10 | 0.008 | 0.53 |
| | $70 < T_{bol} < 200$ K | 18 | 4 | 10 | 4 | 0.00 ± 0.09 | 0.99 | 0.00 |

[a] $N_-$, $N_0$, and $N_+$ are the number of sources in the subsample with normalized velocity difference $\delta V < -0.25$, $-0.25 \leq \delta V \leq 0.25$, and $0.25 < \delta V$, respectively.

[b] Probability of drawing the sample from a zero mean normal parent distribution, based on a Student's $t$-distribution.

[c] The blue excess is defined as $E = (N_- - N_+)/N$.

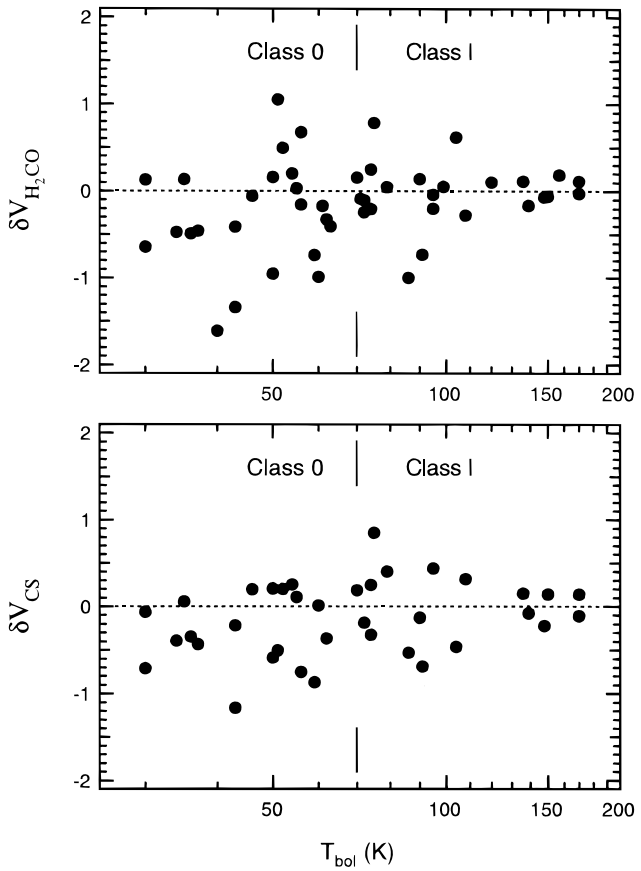


FIG. 4.—The relation between the velocity difference $\delta V$, based on $H_2CO$ (*top*) and CS (*bottom*) as the optically thick line, and the bolometric temperature ($T_{bol}$). Both plots show that most sources have blueshifted values of $\delta V$ at low $T_{bol}$ (class 0 sources). At higher $T_{bol}$ (class I sources), there are an equal number of blueshifted and redshifted sources. The uncertainty in $\delta V$ is typically $\sim 0.05$ km s$^{-1}$ (Table 3), and the uncertainty in $T_{bol}$ is typically of order 20 K (see text).

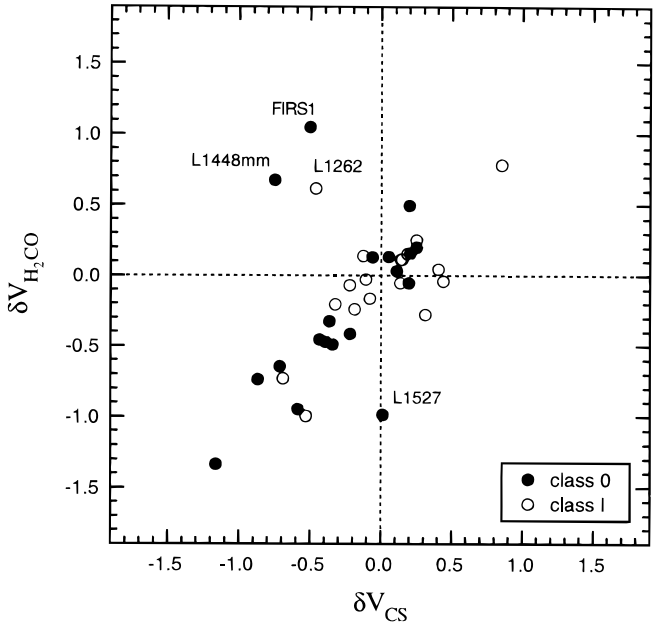


FIG. 5.—The relation between $\delta V$ determined using CS (2–1) and $\delta V$ determined using $H_2CO$ ($2_{12}$–$1_{11}$) as the optically thick lines, and using $N_2H^+$ (101–012) in each case as the optically thin line. Note the good correlation in most sources. The uncertainty in $\delta V$ is typically $\sim 0.05$ km s$^{-1}$ (Table 3), comparable to the symbol size.

sources with $T_{bol} < 70$ K. In this class 0 subsample, the blueshifted excess is $\sim 50\%$, while in the class I subsample, there is no significant blueshifted or redshifted excess.

### 3.4. *Uncertainties Due to Choice of Line and to Angular Resolution*

Our statistical results are significant as long as they are independent of the instruments used, or the lines observed. We compare among different lines to better understand the sources of uncertainty in the statistical results discussed above, in particular the possible effects of chemistry and resolution. We compare the optically thick line profiles of ortho- and para-$H_2CO$, and CS, and the optically thin line profiles of $N_2H^+$ and $C^{34}S$.

#### 3.4.1. *Molecular Tracers as a Source of Uncertainty*

The $H_2CO$ and CS observations give statistically similar results, as shown in § 3.3; we now compare the line profiles individually in each source. The measured peak velocities in the CS (2–1) and $H_2CO$ ($2_{12}$–$1_{11}$) lines agree quite well, as can be seen by inspection of Table 3. Figure 5 plots $\delta V_{H_2CO}$ against $\delta V_{CS}$. Of the 39 sources observed in both lines, four (L1448mm, Serp FIRS 1, L1262, and L1527) deviate significantly from the line of perfect correlation. For the remaining 35, the best-fit line has a slope of $1.05 \pm 0.09$, an intercept of $-0.09 \pm 0.04$, and a correlation coefficient of 0.90. The small differences in the statistics derived above (see Table 5) arise mostly from the different CS and $H_2CO$ lines toward the four discrepant sources mentioned above. A paired *t*-test yields a probability of 0.91 that the means of the CS and $H_2CO$ $\delta V$ distributions are equal, and so we treat both distributions as being drawn from the same parent distribution. We note that the CS and $H_2CO$ velocity differences were normalized by the same $N_2H^+$ line width, and so the correlation in Figure 5 is independent of the normalization.

We observed the $C^{34}S$ (2–1) line toward 11 sources with the SEST and two sources with the IRAM telescope (Table 4). We evaluate the effect of using $N_2H^+$ instead of $C^{34}S$ in order to compute $\delta V$ with CS (2–1) as the thick line. The difference $\delta V_{C^{34}S} - \delta V_{N_2H^+}$ has a mean $\pm$ standard error of the mean (s.e.m.) of $0.06 \pm 0.05$, smaller than the width of one bin in Figure 3. Most of the variation in $\delta V$ comes from the different widths of $C^{34}S$ and $N_2H^+$ in some sources. The $C^{34}S$ lines are broader than the $N_2H^+$ lines by a factor of $1.3 \pm 0.1$. The velocity difference has a mean $\pm$ s.e.m of $0.02 \pm 0.03$ km s$^{-1}$ ($V_{C^{34}S} - V_{N_2H^+}$). Only Serp FIRS 1 and L1251B have $C^{34}S$ velocities differing by more than 0.1 km s$^{-1}$ from the $N_2H^+$ velocity.

Ortho- and para-$H_2CO$ are expected to trace the same physical conditions, and in LTE they are expected to have an ortho/para abundance ratio equal to 3. The observed ortho and para line profiles are very similar in most sources, indicating high optical depth in both lines. In particular, the velocity of the peak is essentially the same in both transitions. The change in $\delta V$ for all 12 sources has a mean $\pm$ s.e.m. of $0.09 \pm 0.05$ (para-ortho), smaller than the width of one bin in Figure 3. The ortho- and para-$H_2CO$ lines have different shapes only toward the sources L483

and VLA 1623, where the ortho-$H_2CO$ line peak velocity is more blueshifted with respect to the $N_2H^+$ velocity than the para-$H_2CO$ line.

#### 3.4.2. *Angular Resolution as a Source of Uncertainty*

We explored the effects of different beam sizes by comparing the IRAM $H_2CO$ line profiles with average profiles over an effective 37″ beam (3 × 3 points with 10″ spacing and 16″ beam) in a sample of 13 sources where we have made maps (Mardones et al. 1997). The self-absorption depth and blue-to-red peak ratio vary somewhat, but the peak velocities are consistent to within 0.1 km $s^{-1}$. The only exception is Serpens FIRS 1, where the red peak is brighter in the IRAM central spectrum, but the blue peak is brighter in the IRAM 3 × 3 average. The difference in $\delta V$ between the average spectrum of the 3 × 3 map and the center spectrum has a mean ± s.e.m. of 0.04 ± 0.03. In general, then, the measured $\delta V$ is not very sensitive to variations in pointing or spatial resolution.

We also compared SEST and IRAM observations in order to study the variation of the line profiles when changing spectral and spatial resolution. The observed SEST line profiles are on average 40% fainter than the corresponding IRAM line profile. This is likely due to beam dilution indicating that the emitting gas is spatially concentrated on scales smaller than the SEST main beam (36″). Some of the sources proved to be very compact as judged by the high IRAM/SEST intensity ratio (notably 16293−2422 and B335). The shapes of the lines observed with both telescopes are very similar in most of the sources, with a few exceptions noted below. For sources with double-peaked $H_2CO$ line profiles, the overall intensity and width of the lines are similar at both telescopes, but the self-absorption depth and the ratio of the two peaks can vary significantly. The dips are always deeper in the IRAM spectra, maybe indicating that the absorption is diluted in the SEST beam also. The peak velocities measured in the SEST and IRAM spectra are consistent with each other. The change in $\delta V$ using the $H_2CO$ velocities measured at the SEST and IRAM has a mean ± s.e.m. of 0.01 ± 0.05 (SEST-IRAM) for the 10 sources in common, excluding Serp FIRS 1. The SEST spectrum toward Serp FIRS 1 is almost identical to the IRAM 3′ × 3′ average spectrum. We find no telescope biases in our observations that could affect the statistics significantly.

## 4. DISCUSSION

We have found an excess of sources with asymmetric, optically thick lines (double-peaked or shoulder profiles) toward a sample of 47 nearby low-mass YSOs. This asymmetry is such that the peak velocity of the optically thick line is preferentially blueshifted with respect to the optically thin velocity. This blueshifted excess is statistically more significant in subsamples of sources with $T_{bol} < 70$ K. The observed blue excess of $\delta V$ values is similar for the CS and $H_2CO$ tracers and is independent of the telescope used. It is, therefore, an inherent property of the sources in the samples.

### 4.1. *Kinematic Interpretation of Observed Velocity Differences*

The observed $N_2H^+$ line profile is single in all sources observed, ruling out multiple components as the cause of the asymmetric lines observed. In a few cases (e.g., L1448mm), the $N_2H^+$ line profile departs significantly from a Gaussian. However, in those cases, the peak of the $N_2H^+$ line profile lies within the $H_2CO$ or CS absorption dip and does not coincide with the peak of the $H_2CO$ or CS profile.

A foreground absorbing layer could reproduce the asymmetric line profiles we observe. However, we do not expect such a layer of dense gas (having the systemic velocity of the source) to lie in front of most of the sources observed unless it is physically associated. On the other hand, the spatial variation of optically thick line profiles shows that the asymmetries are concentrated toward the sources (§ 3.4.2; see also Zhou et al. 1993, Myers et al. 1995, and Mardones et al. 1997), making the casual superposition of two clouds even more unlikely. We are led to explain the variety of line profiles observed as arising from *local* self-absorption, i.e., absorption by physically associated gas.

We now ask what kinematics should the local absorbing gas have with respect to the YSO in order to reproduce the observed $\delta V$ distributions. If the kinematics around a YSO are dominated by infall, then we expect the foreground gas to be preferentially redshifted with respect to the systemic velocity of the source. If this foreground gas has colder excitation temperature than the dense gas in the inner cloud, it will absorb preferentially at redshifted velocities causing asymmetric line profiles (e.g., Leung & Brown 1977; Zhou 1992). Thus, it will have a distribution of $\delta V$ skewed toward blue velocities as observed. If systematic motions are due solely to infall toward a high fraction of class 0 sources, these motions can explain the observed statistics.

The observed blue excess of $\delta V$ can arise from infall, as opposed to expansion, but other motions, including rotation and bipolar outflows, need to be considered. Adelson & Leung (1988) show that rotation can cause infall-like and expansion-like line profiles on either side of the rotation axis (see also Zhou 1995). The observed effect depends on the orientation of the rotation axis with respect to the line of sight. A source sample with randomly oriented rotation axes would produce a symmetric distribution of $\delta V$. Similarly, bipolar outflows also cause infall-like and expansion-like line profiles on either side of the source (Cabrit & Bertout 1986). An ensemble of bipolar outflows with random orientation would also produce a symmetric distribution of $\delta V$, unlike our results. Thus, our statistical results do not rule out the contribution of outflow and rotation to the line profiles, but they require inward motions in addition to any outflow and rotation in a significant fraction of our source sample.

Outflow motions greatly affect the observed line profiles toward some sources, in particular among the class 0 sample. If outflow axes in this sample were not distributed randomly, or if the sample was too small, the outflows could, in principle, produce the observed statistical effect. We now examine on a source-by-source basis whether the observed outflow wings are associated with the excess of sources with blue $\delta V$ in our sample. We subtracted one or two best-fit Gaussians from the $H_2CO$ and CS line peaks in order to measure the remaining blue and red wings in every spectrum. We then labeled each source's wings as blue if the blue wing is greater than 25% brighter than the red, red if the red wing is greater than 25% brighter than the blue, and nil otherwise. We find as many sources with brighter blue and red wings (~25% of each) in both the $H_2CO$ and CS lines, and therefore the excess of sources with negative $\delta V$ *is*

*not* associated with a similar excess of sources with bright blue wings.

To test this further, we defined a wing parameter with values $-1$, 0, or 1 for sources with brighter wings to the blue, neither, or red, respectively, and a line-core parameter with values $-1$, 0, or 1 for sources with a measured $\delta V < -0.25$, $-0.25 < \delta V < 0.25$, or $\delta V > 0.25$, respectively. We find a Spearman rank correlation coefficient between the wing and the line-core parameters of 0.0 for the $H_2CO$ sample and $-0.1$ for the CS sample. We conclude that the observed wing emission is not correlated with, and thus is not responsible for, the excess of sources with negative $\delta V$ derived in § 3.

Finally, it is possible that star-forming groups could have large-scale rotation or magnetic fields imposing a characteristic orientation to the disks and outflows around YSOs. This effect could bias the statistics within each cluster. Evidently this is not the case in this survey, because the projected outflow axes have a wide distribution in position angle within each cluster. The distribution of axis position angles for all outflows with well-known orientation in NGC 1333 has an rms of 56° (Bally, Devine, & Reipurth 1996). Bontemps et al. (1996) found a similar range of outflow axis position angles, with an rms of 55° in Ophiuchus. The position angles of the outflow axes of the Serpens sources S68N, FIRS 1, SMM 2, SMM 4, and SMM 5 have an rms noise of 43° (White, Casali, & Eiroa 1995; Williams et al. 1997). Therefore, within each of the clusters in our survey, we can regard the source outflow axes as randomly oriented.

### 4.2. *Infall toward Class 0 and Class I Sources*

We have shown that the observed distribution of $\delta V$ is explained best by motions that include infall in addition to outflow and/or rotation. Furthermore, we show in § 3.3 that in our sample, the infall signatures are seen almost entirely toward class 0 rather than class I sources. The most straightforward interpretation of these results is that class 0 sources differ from class I sources in having a much greater incidence of inward motions for the conditions that our observations probe—size scales of a few times 0.01 pc and gas density of about $10^5$ cm$^{-3}$. This difference, which has not been demonstrated before, adds support to the idea that class 0 sources have not yet accreted most of their mass, based mainly on the greater submillimeter continuum emission of class 0 rather than class I sources (Andre et al. 1993).

The lack of infall signatures in class I objects, however, does not mean necessarily that infall is absent in these sources. Adams, Lada, & Shu (1987) show that, to model the spectral energy distribution of class I sources, it is necessary to include the contribution of an infalling envelope. The lack of blueshifted line profiles toward class I sources could therefore result from a lower sensitivity of our observations to the physical conditions in the infalling envelopes of class I sources. This would occur if the circumstellar envelopes in class I sources have less optical depth than in class 0 sources, or if the circumstellar envelopes in class I sources have smaller excitation temperature gradients than in class 0 sources (in the optically thick CS and $H_2CO$ lines).

To test the above ideas, we examined the optical depths determined from the multicomponent fits to the $N_2H^+$ spectra for the class 0 and class I sources in our sample. We found no significant difference between the two groups: the $N_2H^+$ optical depth, summed over all seven hyperfine components, has a mean and s.e.m. of $4.9 \pm 0.6$ for the class 0, and $4.6 \pm 0.7$ for the class I source sample. This suggests that the greater incidence of blueshifted profiles in class 0 rather than class I sources does not arise from differences in line optical depth between the two samples. However, the lack of self-absorption features in the class I source line profiles may indicate that the CS and $H_2CO$ optical depths could still be higher in class 0 rather than class I sources. Also, there are more weak, single-peaked sources in the class I than in the class 0 source samples.

Sources whose outflow axes are in the plane of the sky, having edge-on disks, may have significant obscuration to optical and near-infrared radiation, lowering their observed $T_{bol}$. This effect would tend to mix the class 0 and class I sources. However, the circumstellar envelopes are most likely optically thin at submillimeter wavelengths, and so a submillimeter wavelength excess should distinguish class 0 from class I sources, independent of orientation. Among our sample of class 0 sources, only 03282+3035 and L673A have not been detected at submillimeter wavelengths; moving them to the class I sample would only emphasize the observed difference between the class 0 and the class I samples.

Thus, we found a significant difference in the incidence of blueshifted line asymmetry between the class 0 and the class I sources, indicating different physical conditions in the circumstellar envelopes around class 0 and class I sources. However, our observations do not necessarily rule out the presence of inward motions onto class I sources; tracers with higher optical depths may be needed to probe the circumstellar kinematics around class I sources.

### 4.3. *Identification of Infall Candidates*

In Table 6, we summarize the evidence for infall, expansion, or neither for the sources in our sample. We list all 23 sources with $\delta V > 0.25$ in either the $H_2CO$ or CS lines. We label the lines "blue" if they have blue asymmetry ($\delta V < -0.25$), "red" if they have red asymmetry ($\delta V > 0.25$), or "neither" if they have neither ($-0.25 \leq \delta V \leq 0.25$). We include IRAS 13036−7644 in the CS sample, using the spectrum published by Lehtinen (1997). The correspondence between both lines is extremely good, as expected from Figure 5. Following Gregersen et al. (1997), we identify infall candidates as those sources with evidence of infall (at least one "blue") and no evidence of expansion in any line (no "reds"). Therefore, from the $H_2CO$ and CS observations presented in this paper, we select 15 sources as infall candidates: IRAS 03256+3055, NGC 1333-4A, NGC 1333-4B, L1527, IRAS 13036−7644, VLA 1623, WL 22, IRAS 16293−2422, L483, S68N, SMM 5, SMM 4, B335, L1157, and L1251B. These are class 0 sources ($T_{bol} < 70$ K) with the exception of IRAS 03256+3055, WL 22, and L1251B. In contrast to the 15 (CS and $H_2CO$) sources with at least one blue and no reds, there are only four with the opposite property—at least one red and no blues (NGC 1333-2, L1551-5, L1551NE, and L43).

Among our infall candidates, L1527, IRAS 16293−2422, and B335 have been studied widely (e.g., Walker et al. 1986; Zhou et al. 1993, 1994; Mardones et al. 1994; Myers et al. 1995; Ohashi et al. 1997; Gregersen et al. 1997). They represent the best cases for infall to date because of the agreement between kinematic models and observations. The sources NGC 1333-2 (Ward-Thompson et al. 1996), IRAS

TABLE 6

LINE ASYMMETRIES IN SOURCES HAVING $|\delta V| > 0.25$ IN AT LEAST ONE LINE

| SOURCE[a] | $T_{bol}$ (K) | LINE ASYMMETRY[b] | | | |
|---|---|---|---|---|---|
| | | CS (2–1) | $H_2CO$ ($2_{12}$–$1_{11}$) | $HCO^+$ (3–2) | $HCO^+$ (4–3) |
| L1448 mm | 56 | Blue | Red | Red | Red |
| 03256+3055* | 74 | Blue | Neither | ... | ... |
| NGC 1333-2 | 52 | Red | Red | ... | Blue[c] |
| NGC 1333-4A* | 34 | Blue | Blue | Blue | Blue |
| NGC 1333-4B* | 36 | Blue | Blue | Blue | Blue |
| L1551-5 | 95 | Neither | Red | ... | ... |
| L1551NE | 75 | Red | Red | Blue | ... |
| L1527* | 60 | Neither | Blue | Blue | Blue |
| 13036−7644* | 63 | Blue[d] | Blue | ... | ... |
| VLA 1623* | 30 | Blue | Blue | Neither | Neither |
| WL 22* | 86 | Blue | Blue | ... | ... |
| 16293−2422* | 43 | Blue | Blue | Blue | Blue |
| L43 | 79 | Neither | Red | ... | ... |
| L483 | 50 | Blue | Blue | Red | Red |
| S68N* | 40 | Neither | Blue | ... | ... |
| FIRS 1 | 51 | Blue | Red | Red | Blue |
| SMM 5* | 59 | Blue | Blue | ... | ... |
| SMM 4* | 43 | Blue | Blue | Blue | Blue |
| B335* | 37 | Blue | Blue | Blue | Blue |
| L1157* | 62 | Blue | Blue | Blue | Neither |
| L1251A | 108 | Blue | Red | ... | ... |
| L1251B* | 91 | Blue | Blue | ... | ... |
| L1262 | 104 | Red | Blue | ... | ... |

[a] The best cases for infall are indicated with an asterisk.

[b] The line asymmetry is designated "blue" for $\delta V < -0.25$, "neither" for $-0.25 \leq \delta V \leq 0.25$, and "red" for $\delta V > 0.25$. Except where noted, the CS and $H_2CO$ data come from this paper, and the $HCO^+$ line data come from Gregersen et al. 1997.

[c] Ward-Thompson et al. 1996.

[d] Lehtinen 1997.

13036−7644 (Lehtinen 1997), L483 (Myers et al. 1995), S68N (Hurt, Barsony, & Wootten 1996), SMM 4 (Hurt et al. 1996; Gregersen et al. 1997), L1157 (Gueth et al. 1997), and L1251B (Myers et al. 1996) have been identified recently as infall candidates but have not yet been studied as thoroughly as L1527, IRAS 16293−2422, and B335. The sources IRAS 03256+3055, NGC 1333-4A and 4B, VLA 1623, WL 22, and SMM 5 are new kinematic infall candidates based on this work.

### 4.4. *Comparison with Previous Surveys*

Looking for kinematic infall signatures, Wang et al. (1995) observed 12 globules at the CSO using the $H_2CO$ ($3_{12}$–$2_{11}$) line. They do not find convincing spectral evidence of infall toward any source. This may be because none of their sources are known to be class 0 YSOs, or it may be due to the expected lower optical depth of the $H_2CO$ ($3_{12}$–$2_{11}$) line.

Looking for infall signatures, Gregersen et al. (1997) observed 23 class 0 sources in the $HCO^+$ (3–2) and (4–3) lines. Their sample contains sources more distant than 400 pc, but the overlap with our sample is still considerable, with 15 sources in common. We derived $\delta V$ from the $HCO^+$ and $H^{13}CO^+$ spectra presented by Gregersen et al. toward 13 of those sources, and we assigned asymmetry labels blue, red, and neither to them in the same way as for the CS and $H_2CO$ spectra. In Table 6, we list the asymmetry labels from available observations: from this paper, from Gregersen et al. (1997), from Ward-Thompson et al. (1996), and from Lehtinen (1997). The correspondence among all lines is generally good. Seven of the nine sources with infall asymmetry in the $HCO^+$ lines have the same sense of asymmetry in the $H_2CO$ and CS lines. On the other hand, the two sources with expansion asymmetry in the $HCO^+$ lines show infall asymmetry in the $H_2CO$ and/or CS lines (L1448 mm and L483), and one source (NGC 1333-2) shows infall asymmetry in $HCO^+$(4–3) (Ward-Thompson et al. 1996) and expansion asymmetry in CS and $H_2CO$. These disagreements may reflect differing degrees of outflow contamination from one line to the next.

Assuming, as in § 4.3, that the best infall candidates are those sources with evidence of infall in at least one line, and with no evidence for expansion in any line, we consider again the sources in Table 6, now according to their asymmetry in $HCO^+$, as well as in CS and $H_2CO$. Adding this $HCO^+$ data and applying this procedure will remove only one source, L483, from the CS and $H_2CO$ list given in § 4.3, leaving the 14 sources indicated in Table 6 as the best infall candidates. These sources have substantial internal agreement among their asymmetry labels: five have four blues, two have three blues, five have two blues, and two have one blue. At present, these sources have the most evidence of infall from available spectral line surveys, and they have the least evidence against infall.

### 4.5. *Thermal and Turbulent Infall*

The kinematic infall candidates identified in this paper include two sources—B335 and L1527—that exemplify in several ways the "standard model" of low-mass star formation (e.g., Shu, Adams, & Lizano 1987). These sources are relatively isolated and have $NH_3$ line widths dominated by thermal rather than turbulent motions (Myers & Benson

1983; Benson & Myers 1989). Their profiles of $H_2CO$ and other lines are well fitted by radiative transfer models whose kinematics are specified by the "inside-out" mode of collapse of a singular isothermal sphere (Shu 1977).

But these two sources are not representative of the properties of the 15 kinematic infall candidates identified by the CS and $H_2CO$ lines in this paper. Most of these sources differ from the standard model in two ways: their line widths are dominated by turbulent motions, and many of them are found in stellar groups rather than in isolation.

We quantify the turbulent motions of the infall candidates by comparing the FWHM of the optically thin $N_2H^+$ line, given in Table 3, with that expected for gas having equal thermal and nonthermal motions,

$$\Delta V_0 = \sqrt{8 \ln 2 kT \left( \frac{1}{m_{\rm obs}} + \frac{1}{\langle m \rangle} \right)}, \quad (2)$$

where $T$ is the gas kinetic temperature, $m_{\rm obs}$ is the mass of the observed species (29 per amu for $N_2H^+$), and $\langle m \rangle$ is the mean molecular mass (2.3 per amu). For gas with $T = 15$ K, nine out of 15 sources, or 60%, have $N_2H^+$ line widths $\Delta V > \Delta V_0 = 0.57$ km s$^{-1}$, i.e., having greater nonthermal rather than thermal motions. If $T = 10$ K, this fraction increases to 12/15, or 80%. Clearly, most of the kinematic infall candidates have nonthermal motions exceeding their thermal motions.

The nonthermal motions in the $N_2H^+$ line width could arise from motions that appear random to our resolution, which we designate as turbulence, and also from systematic motions, including outflow, infall, and rotation. Since $N_2H^+$ lines (like $NH_3$ lines) tend to trace quiescent core structure (Womack et al. 1992) and do not track outflow maps (Caselli, Benson, & Myers 1997), we expect that the outflow contribution to the $N_2H^+$ line width is relatively small compared with the turbulent component. Similarly, the relative contribution of rotation and infall motions to the optically thin line width is significantly smaller than the random contribution, according to infall models that match the profiles of infall candidates (e.g., Zhou et al. 1993).

To assess the proportion of the infall candidates associated with groups or clusters, we consider those infall sources in the NGC 1333, Ophiuchus, and Serpens clouds, which are associated with a substantial cluster of embedded young stellar objects. Of the 15 infall candidates listed in § 4.3, eight or 53% belong to these three clusters. This accounting is conservative in that we do not count L1251B, which belongs to a smaller group of at least five near-infrared sources (Hodapp 1994). Of these eight sources in clusters, most (six) have $N_2H^+$ line widths dominated by turbulent motions.

This relatively high incidence of turbulent motions and cluster sources in our list of kinematic infall candidates implies that the standard model of isolated star formation in a thermally dominated core is not representative of most of our infall candidates. This is an area where more theoretical models are needed. Models of star formation that account for significant turbulent motions as part of their initial conditions have been presented for a spherically symmetric geometry and for the formation of a single star (Caselli & Myers 1995; McLaughlin & Pudritz 1997), but these models lack a physical basis for the nonthermal motions and do not account for the formation of multiple stars.

### 4.6. *Future Prospects*

The infall candidates identified in this paper are good candidates for the study of star-forming infall. However, it is not established from the survey data presented here that their motions are necessarily either "star forming" or "gravitational."

A further step to establish if the blueshift identified in class 0 sources arises from infalling envelopes is to map them: the blueshifted, asymmetrical line profiles should be spatially concentrated toward the source. Furthermore, maps are needed to disentangle the effects of the outflows. Maps of observed line asymmetry (e.g., Adelson & Leung 1988; Walker et al. 1994) can distinguish whether infall dominates (at low velocities) over rotation or expansion in a given region.

To establish whether the observed infall kinematics are gravitational, the observations should be compared with kinematic models, which predict the spatial variation of the line profiles (e.g., Zhou et al. 1993). Furthermore, continuum observations may help determine the YSO and envelope masses, so as to compare with model predictions. High spatial resolution that is attainable with interferometers can locate the infall regions in relation to the position of the continuum peak of the YSO. All of these together should constrain significantly kinematic models of gravitational collapse, to determine better the physical basis of the inward motions inferred in this paper. In addition, further models and observations may be needed to resolve the apparent conflicts presented in Table 6. Such models will have to incorporate both infall and outflow kinematics.

## 5. CONCLUSIONS

Among 47 of the youngest nearby low-mass PMS stars (spectral classes 0, or $T_{\rm bol} < 70$ K, and I, or $70 \leq T_{\rm bol} \leq 200$ K), a significant fraction show complex line profiles with double peaks or a peak and a shoulder in the optically thick CS (2–1) and $H_2CO$ ($2_{12}$–$1_{11}$) transitions, which trace dense gas ($n > 10^4$ cm$^{-3}$).

These complex spectral profiles are not due to multiple components along the line of sight, since the optically thin $N_2H^+$ (101–012) line, observed toward the same sources, is single. The $N_2H^+$ line velocities are consistent with the $C^{34}S$ (2–1) velocities.

In both CS and $H_2CO$ samples, about half the sources have a significant velocity shift between the optically thick and thin lines.

In both CS and $H_2CO$ samples, there are $\sim$25% more sources whose velocity shift is to the blue rather than to the red. This statistically significant tendency arises entirely from sources with $T_{\rm bol} < 70$ K (class 0 sources). In this class 0 sample, the blueshifted excess is 50% (nine out of 23 for $H_2CO$ and 10 out of 19 for CS), while in the class I subsample, there is no significant blueshifted or redshifted excess.

The observed excess of blueshifts cannot be reproduced by a sample of sources whose kinematics are dominated by either bipolar outflows or rotation, if their symmetry axes are oriented in random directions. On the other hand, infall motions alone, or infall combined with rotation and/or outflows, can explain the excess of blueshifts.

We identify a total of 15 spectroscopic infall candidates, of which six have not been identified previously. Most of these candidates differ from the well-known sources B335

and L1527, which exemplify the "standard model" of an isolated core whose line width is dominated by thermal motions. They tend to have primarily turbulent line widths or are associated with embedded young clusters, or both.

This research was supported by NASA Origins of Solar Systems Program, grant NAGW-3401. Support for this work was provided by NASA through Hubble Fellowship grant HF-01086.01-96A awarded by STScI, which is operated by AURA, Inc., for NASA under contract NAS 5-26555. D. M. thanks the Carnegie Institution of Washington for a Carnegie-Chile Fellowship, and the Government of Chile for a MIDEPLAN Fellowship. M. T. and D. J. W. thank the Harvard-Smithsonian Center for Astrophysics for fellowship support. R. B. and M. T. acknowledge partial support from the Spanish DGICYT grant PB93-48.

REFERENCES

Adams, F. C., Lada, C. J., & Shu, F. H. 1987, ApJ, 312, 788
Adelson, L. M., & Leung, C. M. 1988, MNRAS, 235, 349
Andre, P., Ward-Thompson, D., & Barsony, M. 1993, ApJ, 406, 122
Bachiller, R. 1996, ARA&A, 34, 111
Bachiller, R., Andre, P., & Cabrit, S. 1991, A&A, 241, L43
Bachiller, R., & Pérez, M. 1997, in preparation
Bally, J., Devine, D., Hereld, M., & Rauscher, B. J. 1993a, ApJ, 418, L75
Bally, J., Devine, D., & Reipurth, B. 1996, ApJ, 473, L49
Bally, J., Lada, E. A., & Lane, A. P. 1993b, ApJ, 418, 322
Benson, P. J., & Myers, P. C. 1989, ApJS, 71, 89
Bernes, C. 1979, A&A, 73, 67
Bontemps, S., Andre, P., Terebey, S., & Cabrit, S. 1996, A&A, 311, 858
Bourke, T. L. 1994, MSc thesis, Univ. New South Wales
Bourke, T. L., Hyland, A. R., & Robinson, G. 1995, MNRAS, 276, 1052
Cabrit, S., & Bertout, C. 1986, ApJ, 307, 313
Carballo, R., Wesselius, P. R., & Whittet, D. C. B. 1992, A&A, 262, 106
Casali, M. M., Eiroa, C., & Duncan, W. D. 1993, A&A, 275, 195
Caselli, P., Benson, P. J., & Myers, P. C. 1997, in preparation
Caselli, P., & Myers, P. C. 1995, ApJ, 446, 665
Caselli, P., Myers, P. C., & Thaddeus, P. 1995, ApJ, 455, L77
Chandler, C. J., Gear, W. K., Sandell, G., Hayashi, S., Duncan, W. D., Griffin, M. J., & Hazella, S. 1990, MNRAS, 243, 330
Clark, F. O. 1991, ApJS, 75, 611
Chen, H., Grenfell, T. G., Myers, P. C., & Hughes, J. D. 1997, ApJ, 478, 295
Chen, H., Myers, P. C., Ladd, E. D., & Wood, D. O. S. 1995, ApJ, 445, 377
Choi, M., Evans, N. J., II, Gregersen, E. M., & Wang, Y. 1995, ApJ, 448, 742
Dent, W. R. F., Matthews, H. E., & Walther, D. M. 1995, MNRAS, 277, 193
Devine, D., Reipurth, B., & Bally, J. 1997, in Low Mass Star Formation from Infall to Outflow, Poster Proc. IAU Symp 182, ed. F. Malbet & A. Castets (Grenoble: Obs. Grenoble), 91
Eiroa, C., Palacios, J., Eisloffel, J., Casali, M. M., & Curiel, S. 1997, in Low Mass Star Formation from Infall to Outflow, Poster Proc. IAU Symp 182, ed. F. Malbet & A. Castets (Grenoble: Obs. Grenoble), 103
Fuller, G. A., Lada, E. A., Masson, C. R., & Myers, P. C. 1995, ApJ, 453, 754
Gregersen, E. M., Evans, N. J., II, Zhou, S., & Choi, M. 1997, ApJ, 484, 256
Gueth, F., Guilloteau, S., Dutrey, A., & Bachiller, R. 1997, A&A, in press
Henning, T., Pfau, W., Zinnecker, H., & Prusti, T. 1993, A&A, 276, 129
Hodapp, K. 1994, ApJS, 94, 615
Hurt, R. L., & Barsony, M. 1996, ApJ, 460, L45
Hurt, R. L., Barsony, M., & Wootten, A. 1996, ApJ, 456, 686
Jennings, R. E., Cameron, D. H. M., Cudlip, W., & Hirst, C. J. 1987, MNRAS, 226, 461
Lada, C. J., & Wilking, B. A. 1984, ApJ, 287, 610
Ladd, E. F., Adams, F. C., Casey, S., Davidson, J. A., Fuller, G. A., Harper, D. A., Myers, P. C., & Padman, R. 1991, ApJ, 366, 203
Ladd, E. F., Lada, E. A., & Myers, P. C. 1993, ApJ, 410, 168
Larson, R. 1969, MNRAS, 145, 271
Lehtinen, K. 1997, A&A, 317, L5
Leung, C. M., & Brown, R. L. 1977, ApJ, 214, L73
Lovas, F. J. 1991, J. Phys. Chem. Ref. Data, 21, 181
Mardones, D., Myers, P. C., Caselli, P., & Fuller, G. A. 1994, in ASP Conf. Ser. 65, Clouds, Cores, and Low Mass Stars, Fourth Haystack Conf., ed. D. P. Clemens & R. Barbainis (San Francisco: ASP), 192
Mardones, D., et al. 1997, in preparation
Mauersberger, R., Guelin, M., Martin-Pintado, J., Thum, C., & Cernicharo, J. 1989, A&AS, 79, 217
McCaughrean, M. J., Rayner, J. T., & Zinnecker, H. 1994, ApJ, 436, L189
McLaughlin, D. E., & Pudritz, R. E. 1997, ApJ, 476, 750
Myers, P. C., Bachiller, R., Caselli, P., Fuller, G. A., Mardones, D., Tafalla, M., & Wilner, D. J. 1995, ApJ, 449, L65
Myers, P. C., & Benson, P. J. 1983, ApJ, 266, 309
Myers, P. C., & Ladd, E. D. 1993, ApJ, 413, L47
Myers, P. C., Mardones, D., Tafalla, M., Williams, J. P., & Wilner, D. J. 1996, ApJ, 465, L133
Ohashi, N., Hayashi, M., Ho, P. T. P., & Momose, M. 1997, ApJ, 475, 211
Persi, P., Ferrari-Toniolo, M., Busso, M., Origlia, L., Robberto, M., Scaltriti, F., & Silvestro, G. 1990, AJ, 99, 303
Reipurth, B., Chini, R., Krugel, E., Kreysa, E., & Sievers, A. 1993, A&A, 273, 221
Reipurth, B. 1994, A General Catalogue of Herbig-Haro Objects (Paris: ESO)
Sandell, G., Aspin, C., Duncan, W. D., Russell, A. P. G., & Robson, E. I. 1991, ApJ, 376, L17
Sandell, G., Knee, L. B. G., Aspin, C., Robson, I. E., & Russell, A. P. G. 1994, A&A, 285, L1
Shu, F. H. 1977, ApJ, 214, 488
Shu, F. H., Adams, F. C., & Lizano, S. 1987, ARA&A, 25, 23
Terebey, S., Shu, F. H., & Cassen, P. 1984, ApJ, 286, 529
Walker, C. K., Lada, C. J., Young, E. T., Maloney, P. R., & Wilking, B. A. 1986, ApJ, 309, L47
Walker, C. K., Narayanan, G., & Boss, A. P. 1994, ApJ, 431, 767
Wang, Y., Evans, N. J., II, Zhou, S., & Clemens, D. P. 1995, ApJ, 454, 217
Ward-Thompson, D., Buckley, H. D., Geaves, J. S., Holland, W. S., & Andre, P. 1996, MNRAS 281, L53
White, G. J., Casali, M. M., & Eiroa, C. 1995, A&A, 298, 594
Williams, J. P., Mardones, D., Myers, P. C., & Tafalla, M. 1997, in preparation
Womack, M., Ziurys, L. M., & Wyckoff, S. 1992, ApJ, 387, 417
Wu, Y., Huang, M., & He, J. 1996, A&AS, 115, 283
Yun, J. L., & Clemens, D. P. 1995, AJ, 109, 742
Zhou, S. 1992, ApJ, 394, 204
———. 1995, ApJ, 422, 685
Zhou, S., Evans, N. J., II, Kompe, C., & Walmsley, C. M. 1993, ApJ, 404, 232
Zhou, S., Evans, N. J., II, Wang, Y., Peng, R., & Lo, K. Y. 1994, ApJ, 433, 131